HHS Public Access

Author manuscript

Glia. Author manuscript; available in PMC 2018 April 01.

Published in final edited form as:

Glia. 2017 June ; 65(6): 883–899. doi:10.1002/glia.23132.

E6020, a synthetic TLR4 agonist, accelerates myelin debris clearance, Schwann cell infiltration, and remyelination in the rat spinal cord

Jamie S. Church[1,2], **Lindsay M. Milich**[3], **Jessica K. Lerch**[2,3], **Phillip G. Popovich**[2,3], and **Dana M. McTigue**[2,3]

[1]Neuroscience Graduate Program, The Ohio State University, Columbus, Ohio, USA

[2]Center for Brain and Spinal Cord Repair, The Ohio State University, Columbus, Ohio, USA

[3]Department of Neuroscience, The Ohio State University, Columbus, Ohio, USA

Abstract

Oligodendrocyte progenitor cells (OPCs) are present throughout the adult brain and spinal cord and can replace oligodendrocytes lost to injury, aging, or disease. Their differentiation, however, is inhibited by myelin debris, making clearance of this debris an important step for cellular repair following demyelination. In models of peripheral nerve injury, TLR4 activation by lipopolysaccharide (LPS) promotes macrophage phagocytosis of debris. Here we tested whether the novel synthetic TLR4 agonist E6020, a Lipid A mimetic, promotes myelin debris clearance and remyelination in spinal cord white matter following lysolecithin-induced demyelination. *In vitro*, E6020 induced TLR4-dependent cytokine expression (TNFα, IL1β, IL-6) and NF-κB signaling, albeit at ~10-fold reduced potency compared to LPS. Microinjection of E6020 into the intact rat spinal cord gray/white matter border induced macrophage activation, OPC proliferation, and robust oligodendrogenesis, similar to what we described previously using an intraspinal LPS microinjection model. Finally, a single co-injection of E6020 with lysolecithin into spinal cord white matter increased axon sparing, accelerated myelin debris clearance, enhanced Schwann cell infiltration into demyelinated lesions, and increased the number of remyelinated axons. *In vitro* assays confirmed that direct stimulation of macrophages by E6020 stimulates myelin phagocytosis. These data implicate TLR4 signaling in promoting repair after CNS demyelination, likely by stimulating phagocytic activity of macrophages, sparing axons, recruiting myelinating cells, and promoting remyelination. This work furthers our understanding of immunemyelin interactions and identifies a novel synthetic TLR4 agonist as a potential therapeutic avenue for white matter demyelinating conditions such as spinal cord injury and multiple sclerosis.

Keywords

phagocytosis; oligodendrocyte; macrophage; NG2; demyelination

Correspondence Dana McTigue, 692 Biomedical Research, Tower, 460 W. Twelfth Avenue, Columbus, Ohio 43210, USA., Dana.McTigue@osumc.edu.

James S. Church and Lindsay M. Milich contributed equally to this study.

The authors declare no conflict of interest associated with this work.

1 INTRODUCTION

Myelin is an insulating and energy-providing sheath around axons that is essential for fast conduction velocity and overall axon health and survival. Thus, any loss of myelin can compromise neurological function. Oligodendrocytes (OLs), the myelinating cells of the central nervous system (CNS), are vulnerable to pathological cascades associated with injury, aging, and disease, including oxidative stress, glutamate excitotoxicity, and ischemia. These conditions cause OL loss, which results in demyelination of surviving axons. Under appropriate conditions, OLs can be replaced by endogenous NG2+ oligodendrocyte progenitor cells (OPCs) present throughout the adult CNS; these cells proliferate acutely after demyelination and can differentiate into mature remyelinating OLs (Watanabe, Toyama, & Nishiyama, 2002). Their differentiation, however, is inhibited by myelin debris, a common pathological feature of demyelination and CNS trauma (Boivin et al., 2007; Kotter, Li, Zhao, & Franklin, 2006; Lampron et al., 2015; Neumann, Kotter, & Franklin, 2008; Robinson & Miller, 1999). In these conditions, myelin debris removal is carried out mainly by macrophages derived from microglia and monocytes, which are the principal phagocytes that remove debris after CNS damage (Bruück et al., 1995; Kotter, Zhao, van Rooijen, & Franklin, 2005; Ma et al., 2002; Triarhou & Herndon, 1985; Vallières, Berard, David, & Lacroix, 2006). Therefore, enhancing or accelerating myelin phagocytosis by macrophages is a promising target to promote oligodendrogenesis and remyelination in the demyelinated CNS.

One strategy to enhance phagocytosis is selective activation of toll-like receptor 4 (TLR4) signaling in microglia and macrophages. For instance, systemic treatment with the TLR4 agonist LPS enhanced CNS macrophage activation and accelerated myelin clearance following spinal cord hemisection (Vallières et al., 2006). Additionally, mice deficient in TLR4 signaling displayed reduced myelin phagocytosis after peripheral nerve crush, while microinjecting LPS into the lesion of wild-type mice accelerated myelin debris clearance (Boivin et al., 2007). Previous work from our lab showed that TLR4 activation of macrophages by LPS stimulated myelin debris phagocytosis *in vitro* (Church, Kigerl, Lerch, Popovich, & McTigue, 2016) and that intraspinal microinjection of LPS in the intact rat spinal cord induced robust OPC proliferation and subsequent formation of new OLs (Schonberg, Popovich, & McTigue, 2007).

This study builds on previous work showing that TLR4 activation by LPS promotes repair after demyelinating injuries (Glezer, 2006). Here we tested the ability of the novel TLR4 agonist E6020 to accelerate myelin debris clearance and enhance OL replacement after intraspinal demyelination. E6020 (Eisai Inc., Andover, MA) is a well characterized synthetic Lipid A mimetic with a promising preclinical safety profile (Ishizaka & Hawkins, 2007; Morefield, Hawkins, Ishizaka, Kissner, & Ulrich, 2007). It was developed as a potent nontoxic vaccine adjuvant, in contrast to LPS, which has human toxicity and, since it is a natural product, can have variable potency (Morefield et al., 2007). E6020 is chemically well defined and activates TLR4 but, unlike LPS, does not activate TLR2/6 (Morefield et al., 2007). To date, it has not been tested in the CNS. Thus, here we tested its ability to induce OPC proliferation and OL genesis in the adult CNS as well as tested if it could accelerate myelin debris removal and promote remyelination after demyelination. Our new *in vitro* data

show that treating macrophages with E6020 elicits TLR4-dependent cytokine production and activates intracellular nuclear factor-kappa B (NF-κB) signaling. These indices of macrophage activation are similar to those elicited by LPS but require a 10-fold greater concentration to achieve comparable effects. E6020 also significantly enhanced myelin phagocytosis by macrophages *in vitro*. Intraspinal microinjection of E6020 into the intact rat spinal cord induced macrophage activation, OPC proliferation, and an initial loss of OLs followed by robust OL replacement. Finally, a single intraspinal microinjection of E6020 at the time of lysolecithin-induced demyelination promoted axon sparing, accelerated myelin debris clearance and increased the number of axons myelinated by OLs at 14 days postinjection; surprisingly there was no change OL numbers compared to controls, suggesting that the number of myelin segments per OL was enhanced in the E6020 group. In addition, E6020 treatment significantly enhanced Schwann cell infiltration at day 14 and increased the number of axons remyelinated by Schwann cells 21 days after lysolecithin. This work demonstrates that a single administration of a TLR4 agonist is neuroprotective, boosts macrophage phagocytosis and enhances myelination in the adult CNS, thus highlighting the possibility of manipulating this pattern recognition receptor as a treatment for demyelinating conditions such as spinal cord injury, multiple sclerosis, and other white matter injury or disease.

2 METHODS

2.1 E6020

E6020 was developed and generously donated by Eisai, Inc (Andover, MA). It mimics the physiochemical and biological properties of Lipid A moieties in Gram-negative bacteria and activates TLR4 similar to the natural Gram-negative bacteria TLR4 ligand LPS, although the response is attenuated at equimolar doses (Ishizaka & Hawkins, 2007).

2.2 Bone-Marrow Derived Macrophage Cultures

Bone marrow-derived macrophage cultures were generated as described previously (Longbrake, Lai, Ankeny, & Popovich, 2007) from adult female Sprague Dawley rats or TLR4 deficient (C3H/HeJ) or control (C3H/HeOuJ) mice (Jackson Laboratory, Bar Harbor, ME). Briefly, bone marrow derived macrophages (BMDMs) were obtained from bilateral femurs and tibias using aseptic techniques. Marrow cores were flushed into sterile tubes using syringes fit with 26 gauge needles and filled with Dulbecco's Modified Eagle Medium (DMEM)/10% fetal bovine serum (FBS). Cells were triturated 3–5 times, and red blood cells were lysed in lysis buffer (0.15 M NH_4Cl, 10 mM $KHCO_3$, and 0.1 mM Na_2EDTA, pH 7.4). Cells were washed once in media then plated and cultured in DMEM supplemented with 0.5% gentamicin, 1% glutamax, 1% HEPES, 0.001% β-mercaptoethanol, 10% FBS, and 20% supernatant from sL929 cells. The sL929 (which contains macrophage colonystimulating factor) is needed to promote differentiation of bone marrow cells into macrophages (7–10 days) (Burgess et al., 1985). Cells were replated at 2 million cells per well on day 7 in DMEM media supplemented with 10% FBS, 1% glutamax, and 0.5% gentamicin.

In the first experiment, rat cells were treated with replating media with or without LPS (0.1 μg/mL; Sigma-Aldrich) or E6020 (0.001, 0.01, 0.1, 1, 10, or 100 μg/mL; Eisai) for 24 h. In a second experiment, rat cells were treated with myelin and replating media or E6020 (1 μg/mL) for 2, 4, or 24 hr (see methods below). Mouse TLR4 deficient or control BMDMs were treated with LPS or E6020 for 24 hr and used for RNA isolation (see below). All treatment groups were run in triplicate.

2.3 rtPCR on BMDMs

Exactly 24 hr after stimulation with media, LPS, or E6020, cells were washed twice in sterile phosphate buffered saline (PBS) and mixed in 1 mL cold Trizol (Invitrogen, Carlsbad, CA). Gene-specific primer pairs (Table 1) were used to detect mRNA expression in samples (n = 3 wells/group) via quantitative real-time polymerase chain reaction (Q-RT-PCR). Primer sequence specificity was confirmed with BLAST analysis for highly similar sequences against known sequence databases. Briefly, total RNA was purified from each well (3 wells/treatment) using Trizol and quantified by spectrophotometry. cDNA was prepared from RNA by reverse transcription with SuperScript II and random primers (Invitrogen). PCR reactions were carried out using 10 ng of cDNA, 500 nmol/L of each primer, and SYBR Green master mix (Applied Biosystems, Foster City, CA) in 10 μL reactions. Levels of PCR product were measured using SYBR Green fluorescence collected during Real-Time PCR on an Applied Biosystems 7900 system. Standard curves were generated for each gene using a control cDNA dilution series to check primer efficiency. Melting point analyses were performed for each reaction to confirm single amplified products. Data were calculated using the $\Delta\Delta C_t$ method (Schmittgen & Livak, 2008) and expressed as fold change from media treated cells (gene/18s ratio for uninjured samples equals one). Forward and reverse primer sequences for each gene are listed in Table 1.

2.4 RAW-Blue Cells

RAW-Blue cells (InvivoGen) that had been passaged 12 times and stored in liquid nitrogen were thawed and grown in DMEM media supplemented with 10% FBS, 1% glutamax, and 0.5% gentamicin. Cells were passaged 2× and grown to >80% confluence. Cells were treated with LPS (10, 100, 1000 ng/mL; Sigma-Aldrich, St. Louis, MO) or E6020 (0.001, 0.01, 0.1, 1, 10, or 100 μg/mL; Eisai) made in heat-inactivated FBS containing DMEM media for 24 hr, following which NF-κB/activator protein-1 (AP-1) activation was assessed using QUANTI-Blue according to manufacturer's instructions (InvivoGen, San Diego, CA). All treatment groups were run in triplicate.

2.5 Myelin Isolation & pHrodo Red Dye Labeling

Myelin from the brain of an adult female Sprague Dawley rat was isolated using a modified version of the methods outlined in (Hendrickx, Schuurman, van Draanen, Hamann, & Huitinga, 2014). The whole brain was mechanically dissociated through a 70 μm mesh filter using cold 0.1 M PBS followed by density gradient separation using Percoll (Sigma; GE17-0891-01) of 70, 35, and 0% Percoll in PBS. Myelin was collected from the 0–35% interface, resuspended in 0.32 M sucrose, and further purified using a sucrose gradient (Norton & Poduslo, 1973) of 0.85, 0.32, and 0 M sucrose. Liquid was aspirated and myelin was washed in dH_2O and suspended in 0.1 M PBS pH 7.4.

Myelin concentration was measured using the Pierce BCA protein assay kit (ThermoFisher Scientific, 23225) and labeled with pH-sensitive dye pHrodo red, succinimidyl ester (ThermoFisher Scientific, P36600) dissolved in dimethyl sulfoxide (DMSO). Myelin was suspended in 0.1 M PBS pH 8.4 and incubated with 0.1 mM dye at room temperature for 45 min. Myelin + dye was spun and resuspended in 0.1 M PBS pH 7.4 and stored at −80°C until used.

2.6 Phalloidin Immunofluorescence

BMDM morphology was visualized using Phalloidin staining with Hoechst nuclear stain. Fixed cells were washed in 5%FBS/PBS, permeablized with 0.2%Triton X-100, and incubated with Alexa Fluor Phalloidin 488 (1:1000, ThermoFisher Scientific, A12379) for 3 hr at room temperature. Cells were washed and treated with Hoechst (1:50,000) for 5 min and left in PBS. Images were obtained at 20× magnification using the Thermo Scientific ArrayScan XTI.

2.7 Myelin Phagocytosis Analysis of BMDMs

Cells were identified as BMDMs if they were Hoechst and Phalloidin positive. Phalloidin positive BMDMs were determined by thresholding against the background intensity in nonstained wells. The average Phalloidin intensity was at least 3 times the background intensity. Hoechst positive cells that were Phalloidin negative were excluded from analysis. BMDM myelin uptake was determined by thresholding the myelin intensity against the background intensity in nontreated BMDM wells. A BMDM that had taken up myelin was at least 3 times the maximum background intensity in the nontreated wells. The presence of myelin was quantified using the ArrayScanXTI Spot Detector Algorithm (ThermoFisher). 250 Hoechst/Phalloidin+ cells were analyzed per well for their myelin content. The percentage of cells containing myelin was determined for BMDMs that received either media or E6020 (1 μg/mL) treatment for 2, 4, or 24 hr. Three or four wells per treatment were analyzed and averaged.

2.8 Microinjections

Adult female Sprague Dawley rats (250 g) were anesthetized with ketamine (80 mg/kg i.p.) and xylazine (10 mg/kg i.p.). A laminectomy was performed at the T8 vertebral level using aseptic technique. A glass micropipette (custom pulled and beveled to an external tip diameter of 30–40 μm) was inserted 0.7 mm lateral to midline and 1.1 mm ventral to the surface of the exposed cord. A pneumatic picopump (DKI, Tujunga, CA) was used to inject 500 nL of E6020 (10 mg/mL; Sigma-Aldrich) or vehicle (0.1 M PBS) (n = 4/group) into rats randomly assigned to treatment groups. After injection, the micropipette remained in place for 3 min to prevent backflow; the micropipette was then slowly removed, and the injection site was marked with sterile charcoal (Sigma-Aldrich). The musculature surrounding the laminectomy was sutured, the skin was closed with wound clips, and each rat was given 5 mL of saline before being placed in warmed recovery cages.

2.9 Lysolecithin

A laminectomy at T8 vertebral level was performed as described above. A double-barreled micropipette (custom made and beveled to a total external tip diameter of 60 μm) was inserted 0.9 mm lateral to midline and 1.1 mm ventral to the surface of the exposed cord to target lateral white matter. A pneumatic picopump was used to inject 500 nL of lysolecithin (1%; L-α-Lysophosphatidylcholine from egg yolk ≥99%; Sigma-Aldrich) through one pipette tip then 500 nL of E6020 (10 mg/ mL) or vehicle (0.1 M PBS) through the second pipette tip; rats were randomly assigned to the E6020 or vehicle groups. After the second injection, the micropipette remained in place for 3 min to prevent back-flow; the micropipette was then slowly removed, and the injection site was marked with sterile charcoal (Sigma-Aldrich). The musculature surrounding the laminectomy was sutured, the skin was closed with wound clips, and each rat was given 5 mL of saline before being placed in warmed recovery cages.

2.10 BrdU

To label proliferating cells, the thymidine analog 5-bromo-2′-deoxyuridine (BrdU; 50 mg/kg in sterile saline; Sigma-Aldrich) was injected intraperitoneally (i.p.) 1, 2, and 4 hr after surgery in animals surviving 1 day, or 1 hr after surgery and once a day up to 7 days until sacrifice in animals surviving 7 days for microinjection studies.

2.11 Tissue Processing

Naïve rats were sacrificed at 1 or 7 days after microinjection of PBS or E6020 (n = 3–4/ group). Rats receiving lysolecithin and PBS or E6020 co-injection were sacrificed at 3, 7, 14, or 21 days (n = 4–5/group). All rats were anesthetized with a lethal cocktail of ketamine/ xylazine (1.5× surgery dose) and transcardially perfused with 0.1 M PBS followed by 4% paraformaldehyde (PFA). Spinal cords were dissected and postfixed in 4% PFA for 2 hr, transferred to 0.2 M phosphate buffer overnight, and then cryopreserved in 30% sucrose solution in tap water for 3 days. Frozen spinal cords were blocked into 6 mm segments centered on the injection site then embedded in Tissue-Tek optimum cutting temperature medium (VWR International, West Chester, PA). Serial cross-sections (10 μm) were cut through each block using a Microm cryostat (HM 505 E) then were collected on SuperFrost Plus slides (Fisher Scientific, Fair Lawn, NJ) and stored at −20°C

Additional rats microinjected with lysolecithin and PBS or E6020 (n = 5/group) were perfused 14 days after injection with PBS followed by 4% paraformaldehyde/2% gluteraldehyde solution. Spinal cords were removed, and 1 mm segments of tissue at the injection site and rostral and caudal were blocked. Tissue was processed for Epon embedding and semithin sections cut at 1 μm in a transverse orientation on an ultramicrotome (Ultracut MZ6, Leica Microsystems, Austria). Sections were stained with 1% toluidine blue, dipped in histoclear, and coverslipped.

2.2 Immunohistochemistry

Microinjection sites were identified as the section with greatest CD11b immunoreactivity. In most cases needle tracts were evident with CD11b immunoreactivity. Lysolecithin

demyelination lesion epicenters were determined as the area with the greatest demyelination determined with eriochrome cyanine (EC)/neurofilament (NF) immunostaining.

For tissue analysis, the following targets were visualized using immunohistochemistry: rabbit anti-NG2 (1:200; Millipore, Billerica AB5320); mouse CC1 (antibody clone for oligodendrocytes, also called adenomatous polyposis coli (APC), 1:800; Abcam, Cambridge, UK, ab16794); mouse anti-CD11b for microglia and macrophages (1:2000; OX42 clone; Serotec, Raleigh, NC); rabbit anti-Iba1 for microglia and macrophages (1:500; Wako, Japan, 019–19741); rabbit anti-glial fibrillary acidic protein (GFAP) for astrocytes (1:4000; Dako, Santa Clara, CA Z0334); mouse anti-NF for axons (1:2000; Developmental Studies Hybridoma Bank [DSHB], RT97); rabbit anti-p75 for immature non-myelinating Schwann cells (1:1000; Promega, Madison, WI G323A); chicken anti-P0 for Schwann cell myelin (1:500; Aves, Tigard, OR PZ0), and mouse anti-BrdU (1:200, G3G4; DSHB) or biotinylated sheep anti-BrdU (1:200; abcam, ab2284) for proliferating cells. To double-label axons and myelin, NF immunohistochemistry was combined with EC, which labels myelin. For this procedure, sections were rinsed in distilled water and treated with acetone for 5 min. Next, sections were sequentially incubated in EC solution for 30 min in the dark, 5% iron alum for 3 min, and then a borax-ferricyanide solution for 1 min. For BrdU immunohistochemistry, sections were denatured in 2N HCl at 37°C for 25 min before primary antibody incubation. CC1/GFAP labeled sections were counterstained with methyl green. Immunofluorescence was used to identify CC1/BrdU+ cells using Alexa Fluor 546 antimouse secondary antibody (1:1000; Molecular Probes, Eugene, OR) for CC1 cells and Alexa Fluor 488 anti-mouse secondary antibody (1:1000; Molecular Probes, Eugene, OR) for BrdU; and CD11b/Iba1+ cells using Alexa Fluor 546 anti-mouse secondary antibody (1:500; Molecular Probes, Eugene, OR) for CD11b cells and Alexa Fluor 488 anti-rabbit secondary antibody (1:500; Molecular Probes) for Iba1 cells.

Sections were rinsed in 0.1 M PBS and blocked for nonspecific antigen binding using 4% bovine serum albumin/0.1% Triton X-100/ PBS (BP+) for 1 hr. Next, sections were incubated in primary antibody overnight at 4°C. Sections were rinsed and treated with biotinylated antiserum in BP+ (horse anti-mouse IgG 1:800; goat anti-rabbit 1:2000; Vector Laboratories, Burlingame, CA) for 1 hr at room temperature. After rinsing, endogenous peroxidase activity was quenched using a 4:1 solution of methanol/30% hydrogen peroxide for 15 min in the dark. Sections were then treated with Elite avidinbiotin enzyme complex (Vector Laboratories) for 1 hr. Visualization of labeling was achieved by using either SG or 3,3-diamino-benzidine (Vector Laboratories). Sections were rinsed, dehydrated, and coverslipped with Permount (Fisher Scientific, Pittsburgh, PA). Fluorescent slides were treated with a high salt solution before secondary antibody incubation. Following incubation they were incubated with DAPI (1:50,000) to label cell nuclei, washed in dH_2O, and coverslipped in Immu-Mount (Fisher).

2.13 Oil Red O Staining

Oil red O staining was performed to visualize lipid accumulation in the lysolecithin treated sections. Tissue sections were placed in 70% ethanol for 10 min before being placed in a saturated solution of Oil red O (Sigma-Aldrich, O0625-25G) (dissolved in 70% ethanol at

60°C) for 30 min. The tissue was differentiated in ethanol, washed in distilled water, and then coverslipped with Immu-Mount (Fisher).

2.14 Lesion Size Analysis

EC/NF labeling was used to determine lesion size following lysolecithin demyelination. Lesion size was determined as the scan area (mm^2) of all demyelinated tissue (no EC) within the microinjection site cross-section.

2.15 Proportional Area Analysis

To obtain activated microglia/macrophage density, images were digitized and manually outlined using image analysis software (MCID Elite, Imaging Research Inc., Canada). For the initial microinjection study, the entire ipsilateral half was quantified; in lysolecithin treated tissue analysis was confined to the lesioned area (determined by EC/NF). The proportional area of activated macrophages was calculated by dividing the area immunoreactive for CD11b by the scan area. Areas of missing tissue were excluded from this and all analyses.

For lysolecithin treated rats, intraspinal lipid accumulation was analyzed using the proportional area of oil red O staining normalized to the lesion scan area outlined using EC/NF staining. The trace of core lesion area outlined was overlaid on oil red O stained cross-sections, and positive staining was analyzed within that region.

2.16 Cell Density Quantification

Cells immunoreactive for NG2+/BrdU+, CC1+/GFAP−, and p75+ were manually counted at 40×. The criteria to count single-labeled or double-labeled cells included each profile having a well-defined border surrounding an identifiable nucleus. A cell was only counted if both criteria were met in the same plane of focus. Cell type was verified at higher power (64×) when needed. NG2+ macrophages or pericytes were excluded based on morphological criteria. NG2+ progenitors have a multipolar or bipolar morphology and cell surface labeling around the nucleus, versus thin surface labeling distant from the nucleus on macrophages, and labeling of crescent shaped morphology without processes located adjacent to vasculature on pericytes (McTigue, Wei, & Stokes, 2001). Any CC1+ cell that also expressed GFAP was excluded. In the microinjection study, all cells in the ipsilateral half of the section were counted. In tissue injected with lysolecithin, analysis was confined to the demyelinated lesion (determined by EC/NF). Cells immunofluorescent for CC1/BrdU were counted at 20× with 2× zoom using confocal microscopy (Olympus FV 1000 Filter confocal microscope) in optical sections (<1 μm). Bilateral sample boxes (0.0961 mm^2) were placed in the gray matter and lateral white matter adjacent to the injection site. For all cell counts, data are expressed as cells per mm^3.

2.17 P0 Myelin Ring Quantification

Complete P0 Schwann cell myelin rings were manually counted at 63× in the ipsilateral spinal cord at 21 days postlysolecithin. Three tissue sections 150 μm apart, including injection sites, were counted and averaged to obtain one value per animal.

2.18 Remyelinated Axon Quantification

At 14 days after lysolecithin injection, thinly myelinated (indicative of OL myelin) and bare axons just within the lysolecithin lesion border were systematically counted at 100× in semithin plastic tissue stained with toluidine blue. Within each lesion, a sample box (5898.5 μm^2) was placed just inside the medial, lateral, ventral, and dorsal edges of the lesion for a total of four sample boxes per section. The number of thinly myelinated and bare axons from the four sample boxes was summed to obtain one value per section. Three sections per animal were averaged to obtain one value for thinly myelinated and bare axons per animal.

To verify axon remyelination, a subset of tissue blocks was trimmed to the region of interest, and 80 nm thin sections were cut using a diamond knife on a Leica EM UC6 ultra-microtome. Thin sections were collected on 200 mesh copper grids and stained with 1% uranyl acetate and Reynold's lead citrate. Observations were made on an FEI Tecnai G2 Biotwin TEM operating at 80 kV and micrographs captured using an AMT camera.

2.19 Data Analysis

All data collection was performed in a blinded manner, and data are represented as mean ± SEM. PCR data of BMDMs were analyzed by one-way ANOVA. *Post-hoc* analyses included two-tailed t test between media and LPS to confirm effect of LPS, and Dunnett's test of E6020 doses compared to LPS. Myelin uptake by BMDMs was analyzed by two-way ANOVA with Bonferroni's post-hoc analysis. QUANTI-Blue assay of RAW-Blue cells was analyzed by one-way ANOVA with Dunnett's *post hoc* compared to media. CD11b, NG2/BrdU, CC1/GFAP, EC/NF, and ORO analyses were analyzed by two-way ANOVA with Bonferroni's *post hoc* analysis for microinjection and lysolecithin studies. CC1/BrdU cell counts were analyzed by two-way repeated measures ANOVA with Bonferroni's *post hoc* analysis. p75 cell counts, P0 myelin ring counts, and remyelinated fibers were analyzed by two-tailed *t* test.

3 RESULTS

3.1 E6020 Activates Macrophages, Induces Cytokine Production, and Signals through NF-κB *In Vitro*

Macrophages respond to the TLR4 ligand LPS with cytokine production and activation of NF-κB. Here we sought to identify a concentration of the synthetic TLR4 agonist E6020 that produced a similar response in BMDMs to a commonly used dose of LPS (0.1 μg/mL) *in vitro*. Rat BMDMs were treated for 24 hr with DMEM media, LPS, or E6020 then inflammatory gene expression was analyzed using rtPCR.

As expected, LPS (0.1 μg/mL) activated BMDMs, significantly increasing their expression of tumor necrosis factor alpha (TNFα), interleukin (IL) 1β, and IL-6 (Figure 1a–c). E6020 also increased expression of these cytokines in a dose-dependent manner, with ~10-fold reduced potency compared to LPS (Figure 1a–c). These data indicate that, although less potent than LPS, E6020 activates macrophages, mimicking effects of TLR4 activation previously described using blood mononuclear cells (Ishizaka & Hawkins, 2007). Here, the reduced potency of E6020 versus LPS at the same concentration supports previous findings

of reduced cytokine expression with equimolar doses of E6020 and LPS (Ishizaka & Hawkins, 2007). Verification that E6020 works specifically through TLR4 was obtained using mouse macrophages deficient in TLR4 signaling. This revealed that while E6020 induced TNFα, IL-1β, and IL-6 mRNA in wild type mouse macrophages as expected, macrophages lacking TLR4 signaling were completely unresponsive to E6020 (and LPS; data not shown).

E6020 is reported to activate NF-κB (Ishizaka & Hawkins, 2007). To confirm this response in our hands, RAW-Blue Cells were treated with DMEM media, or varying concentrations of LPS or E6020 for 24 hr. This macrophage reporter cell line secretes an embryonic alkaline phosphatase inducible by NF-κB that can be measured using QUANTI-Blue medium. As expected, LPS treatment significantly increased NF-κB activation compared to media. E6020 treatment also significantly increased NF-κB activation, again with ~10-fold less potency than LPS (Figure 1d).

Phalloidin staining of activated macrophages revealed an obvious morphological transformation in LPS- and E6020-activated macrophages. At rest, unstimulated macrophages displayed bright phalloidin immunoreactivity with compact round or bipolar morphology (Figure 1e). LPS and E6020 both induced an activated morphology, with the majority of macrophages displaying large, round cell bodies 24h after treatment (Figure 1f,g). Taken together, these data verify that E6020 activates TLR4 on macrophages *in vitro*, enhancing their ability to produce NF-κB-regulated cytokines.

3.2 E6020 Microinjection Activates Macrophages in the Intact Spinal Cord

Previous work showed that microinjection of the TLR4 agonist LPS into the rat spinal cord white matter/gray matter border induces macrophage activation, especially within the gray matter (Schonberg et al., 2007). We tested whether microinjecting E6020 also activates macrophages *in vivo*. Microinjection of E6020 (1 μg/mL) at the white matter/gray matter border activated intraspinal macrophages. At day 1 postinjection, small rounded macrophages were present throughout the ipsilateral gray and white matter, with the majority of cells concentrated in an ellipse in the lateral white matter (Figure 2a). The area occupied by activated macrophages increased by 7 days, most notably in the white matter, in contrast to vehicle-injected cords which displayed no macrophage activation at either time (Figure 2b, c). Quantification of CD11b immunoreactivity verified that macrophage activation increased significantly between 1 and 7 day after intraspinal E6020 microinjection (Figure 2d). Double-labeling with Iba1 confirmed the macrophage phenotype of the CD11b + cells (data not shown).

3.3 OPCs Proliferate and New OLs Are Formed in E6020 Injection Sites

Intraspinal LPS injection into the intact adult rat spinal cord induces OPC proliferation around the injection site by day 3 and subsequent OL genesis by day 7 (Schonberg et al., 2007; Schonberg & McTigue, 2009). Here we tested whether E6020 had a similar effect. Proliferating OPCs (BrdU+/NG2+), OL numbers (CC1+), and new OLs (BrdU+/CC1+) were counted ipsilateral to the microinjection sites.

Few OPCs incorporated BrdU at any time in vehicle-treated cords (Figure 3a,b). In contrast, E6020 significantly increased OPC proliferation over 7 days (Figure 3a,c). BrdU+ NG2 cells were present throughout the ipsilateral spinal cord, with most concentrated in the lateral white matter surrounding the area of greatest macrophage activation.

TLR4 activation of microglia by LPS can induce OL death in mixed glial cultures and after intracerebral injection (Jeong, Ji, Kim, Jou, & Joe, 2013; Lehnardt et al., 2002; Zhang, Yao, Whetsell, & Sriram, 2013). Our laboratory has also noted significant OL loss 1 day after intraspinal LPS injection (personal observation) followed by robust OL genesis and increased OL numbers 1 week later in adult rats (Schonberg et al., 2007). To determine if E6020 affects OL loss or replacement, spinal cords were examined at day 1 and day 7 postinjection (Figure 4a,b). Vehicle injections had no effect on OLs at either time (Figure 4a,c). E6020 microinjection significantly reduced OL numbers by day 1 post-injection, most notably in the region of robust macrophage activation (Figure 4c; it should be noted as well that on occasion E6020 caused robust macrophage activation in gray matter, which was associated with neuron loss in addition to OL loss at day 1). However, by day 7, OL number in E6020-injected tissue had increased >6-fold, resulting in ~40% more OLs compared to controls (Figure 4b,c). To verify that this response was due to new OL formation, BrdU+/CC1+ cells were quantified at day 7. Compared to controls, E6020-treated spinal cords had significantly more new OLs in the gray matter and white matter (Figure 4d). Collectively, these data demonstrate that intraspinal TLR4 activation by E6020 induced an initial loss of OLs, followed by robust OPC proliferation and widespread OL genesis.

3.4 E6020 Does Not Increase Lesion Size following Lysolecithin-Induced Demyelination

Next, the ability of TLR4 activation via E6020 to enhance remyelination in the CNS was tested. For this, lysolecithin was injected into the intact rat spinal cord, which induces transient demyelination followed by spontaneous remyelination within 5 weeks (Hall, 1972; Blakemore, 1976). Macrophage depletion impairs remyelination after intraspinal lysolecithin (Kotter, Setzu, Sim, van Rooijen, & Franklin, 2001), revealing an essential role for macrophages in myelin repair. However, given that TLR4 activation causes acute OL loss, it is possible that activating TLR4 concomitant with lysolecithin would exacerbate lesion formation and alter repair. To examine this, lysolecithin was co-injected with vehicle or E6020 into the intact spinal white matter in adult rats. The area of demyelination was quantified based on myelin (EC) and axon (neurofilament) double-labeling at 3–21 days postinjection. At all times examined, the demyelinated area in E6020-treated tissue was comparable to controls (Figure 5a,b,g), revealing that TLR4 activation at the time of demyelination did not enhance lesion size.

3.5 TLR4 Activation with E6020 Accelerates Macrophage Activation after Demyelination

Data above show that E6020 microinjection induces rapid and robust macrophage activation (see Figure 2). Thus, next we assessed if E6020 treatment increased macrophage activation over that induced by lysolecithin in demyelinated lesions. Injection of lysolecithin plus vehicle or E6020 both elicited macrophage activation in the lesions; macrophages were distributed throughout the demyelinated zone at day 3 and formed dense clusters by 7–14 days after injection (Figure 5c,d). However, E6020 accelerated the macrophage response, as

these sections contained significantly more macrophage immunoreactivity at day 7 compared to controls, which had not changed from day 3 (Figure 5h). Macrophage reactivity robustly increased in control tissue between 7 and 14 days, at which time lesions co-injected with vehicle had significantly more macrophage reactivity compared to E6020 (Figure 5h). Double labeling of CD11b and Iba1 confirmed these cells were macrophages (data not shown).

3.6 E6020 Accelerates Myelin Debris Clearance in Demyelination Lesions

Data from various injury models implicate TLR4 activation in promoting myelin debris clearance from demyelinated regions (Boivin et al., 2007; Li, Zhang, Zhang, Wen, Lu, & Shen, 2014; Vallières et al., 2006). Here, the ability of E6020 to accelerate or enhance myelin debris phagocytosis in the demyelinated lesions was tested. Oil red O (ORO) stain was used to label phagocytosed myelin debris (Ma et al., 2002).

After lysolecithin plus vehicle injection, few ORO+ lipid droplets were present in phagocytic cells at 3–7 days; these increased significantly by 14–21 days postinjection in the control cords (Figure 5e,i), which closely matches the time course of macrophage activation in this group. ORO labeling in E6020 treated tissue was similar to vehicle at day 3 but was significantly increased by day 7 (Figure 5f,i). This high level of lipid debris was eliminated by 14 and 21 days postinjection, resulting in ORO levels significantly lower than that in the lysolecithin plus vehicle group (Figure 5f,i). These data demonstrate that TLR4 activation via E6020 robustly accelerates myelin debris phagocytosis and degradation following lysolecithin-induced demyelination.

To verify that E6020 directly stimulates myelin phagocytosis by macrophages, rat BMDMs were co-stimulated *in vitro* with myelin and media or E6020 for 2, 4, or 24 h. Myelin was tagged with pHrodo red, a dye that fluoresces in acidic environments, such as macrophage lysosomes. Using this technique, the number of macrophages containing phagocytosed myelin was quantified. In myelin plus vehicletreated BMDMs, ~13% had phagocytosed myelin by 2 hr, which rose to ~25% at 4 hr and slightly declined by 24 hr (Figure 6a,b). Treatment with E6020 significantly increased the number of myelin-containing macrophages at 2 and 24 hr, compared to controls (Figure 6a). Indeed, almost 50% of macrophages treated with E6020 had taken up myelin by 2 hr (47%, Figure 6a,c), which increased further by 24 hr when over 70% of TLR4-activated macrophages had phagocytosed myelin (Figure 6a,c). Similar to above (Figure 1), E6020 treatment induced a larger, rounded morphology by 24 hr (Figure 6d). These data provide evidence that TLR4 activation directly enhances myelin debris uptake by macrophages and suggests a potential mechanism of E6020-mediated acceleration of myelin debris clearance from the intraspinal demyelinated lesions.

3.7 E6020 Increased Axon Survival after Lysolecithin and Enhanced OL Remyelination but Not OL Formation

Lysolecithin is a demyelinating detergent that typically causes minimal direct damage to axons (Hall & Gregson, 1971; Hall, 1972). Remyelination of bare axons may begin as early as day 7 in rodents with near complete remyelination by 3–5 weeks (Blakemore, 1976; Jeffery & Blakemore, 1995). Because E6020 treatment accelerated myelin debris

phagocytosis, we hypothesized that remyelination also would occur earlier. In semithin plastic sections prepared 14 days after injection of lysolecithin plus E6020 or vehicle, sample boxes were used to quantify bare and thinly myelinated axons indicative of OL remyelination. Unexpectedly, lesion cores were mostly void of axons and instead were filled with macrophages in both groups (Figure 7a,b). Therefore, axon counts were restricted to just within lesion borders where both groups contained axons. As expected, control lysolecithin lesions contained a subset of axons with thin myelin indicative of OL remyelination. Strikingly, E6020-treated tissue had significantly more axons overall, including more bare axons and more axons wrapped with thin OL myelin (Figure 7c – e). Thus, TLR4 activation concomitant with lysolecithin treatment limited axonal loss and supported oligodendrocyte remyelination.

To determine if the greater number of remyelinated axons in E6020 lesions correlated with an increase in OLs, the number of OLs within lysolecithin lesions was counted at 14 and 21 days postinjection. Interestingly, OL numbers were comparable in both groups at each time (Figure 8a – c), revealing that although there was more OL remyelination at day 14, E6020 did not alter the timing or extent of OL replacement after lysolecithin.

3.8 TLR4 Activation via E6020 Increased Schwann Cell Recruitment and Myelin Production in Intraspinal Demyelination Lesions

Upon inspection of the 14 day epon-embedded sections, it was clear that many bare axons had a one-to-one association with cells resembling Schwann cells. Indeed, it has been known for over 30 years that Schwann cells contribute to remyelination in the CNS following chemical demyelination (Blakemore, 1976; Blakemore, Eames, Smith, & McDonald, 1977; Graça & Blakemore, 1986). To examine Schwann cell infiltration into the lesions, 14 day postinjection sections were immunolabeled for p75, which is expressed by nonmyelinating Schwann cells, and the number of p75+ cells was quantified in a blinded manner. While both treatment groups contained p75 + Schwann cells at 14 days postinjection, E6020 treatment doubled the number of p75+ cells compared to vehicle ($p < .05$; Figure 8d–f).

To determine if Schwann cells myelinate axons in the lysolecithin lesions, 21 day postinjection sections were immunolabeled for P0, a protein restricted to Schwann cell myelin. The number of P0+ myelin rings within the lesions was counted, which revealed that the number of Schwann cell myelinated axons after E6020 treatment was significantly greater than controls (Figure 8g–i). These data show, for the first time, that intraspinal TLR4 activation concomitant with lysolecithin is protective to axons, increases the number of Schwann cells in the CNS following demyelination, and enhances their contribution to endogenous remyelination.

4 DISCUSSION

This work demonstrates that E6020, a synthetic Lipid A mimetic and TLR4-specific agonist, enhances macrophage phagocytosis and accelerates repair after intraspinal demyelination. *In vitro*, E6020 treatment of macrophages induced cytokine production, intracellular NF-κB signaling, and a round “activated” morphology. In comparison to LPS, E6020 was less potent, as expected, but still produced the same general activated phenotype (Ishizaka &

Hawkins, 2007). For LPS to activate and signal through TLR4, additional co-stimulatory molecules are required, including LPS binding protein (LBP), lymphocyte antigen 96 (MD2), and cluster of differentiation 14 (CD14) (Lu et al., 2008). E6020, however, does not require CD14 and whether MD2 is necessary for its activation of TLR4 signaling is unknown (Ishizaka and Hawkins, 2007). Recently, the importance of CD14 in conferring and heightening LPS sensitivity and regulating inflammatory function in microglia was reported (Janova et al., 2015). Perhaps lack of CD14 involvement in E6020 activation of TLR4 contributes to its decreased potency. The elevated inflammatory response of macrophages to increasing doses of E6020 demonstrates a wide range of sensitivity to this TLR4 agonist, and thus the potential to finely tune macrophage function *in vitro* and *in vivo*.

Previously, our group showed that intraspinal LPS injection activates macrophages and enhances OPC proliferation and OL genesis (Schonberg et al., 2007). Here we show that intraspinal E6020 injection produces similar effects. Interestingly, despite the fact that injections of both LPS and E6020 were made into the gray/white matter border, there were subtle but important differences in the magnitude and location of the macrophage reaction. With both TLR4 agonists, cells with round activated morphology were present throughout the ipsilateral cord; however, macrophage activation was greatest in the lateral white matter after E6020 microinjection whereas LPS caused focal activation of dense macrophage clusters in gray matter. Because E6020 does not contain the saccharide scaffold of LPS and other synthetic TLR4 agonists (Ishizaka & Hawkins, 2007), its lipophilic nature may preferentially allow it to accumulate in the white matter. Thus, comparable injections of LPS, which cause the greatest macrophage response in the gray matter (Schonberg et al., 2007), create focal zones of dense macrophage activation with significant neuron loss (Jeong et al., 2013). E6020 did not cause neuron loss, except in the occasional injections that elicited a small but robust macrophage response in gray matter. Thus, differences in the diffusion characteristics of these TLR4 agonists may create focal zones of activated macrophages with more/less neurotoxic potential. Alternatively, differences in accessory molecules involved in TLR4 signaling between LPS and E6020 (discussed above) may alter the migration or phenotype of activated macrophages to preferentially accumulate near neuron cell bodies and areas of dense vasculature or white matter tracts, respectively. For example, CD14 (required for LPS but not E6020 signaling via TLR4) enhanced macrophage recruitment and infiltration in an abdominal aortic aneurysm induction model (Blomkalns et al., 2013). Furthermore, dopamine increases CD14+ monocyte adherence and migration within the brain (Coley, Calderon, Gaskill, Eugenin, & Berman, 2015), and dopaminergic projections within the spinal cord terminate in gray matter (Lindvall, Bjoörklund, & Skagerberg, 1983). Therefore, in addition to diffusion properties, TLR4 co-signaling molecules may determine the magnitude and localization of LPS versus E6020 mediated macrophage activation within the spinal cord.

E6020 microinjection into the uninjured spinal cord caused acute OL loss, followed by OPC proliferation and OL genesis over 7 days, primarily around the area of greatest macrophage activation. *In vitro* work shows LPS activated microglia are toxic to OL lineage cells (Pang, Cai, & Rhodes, 2000; Lehnardt et al., 2002; Pang et al., 2010), potentially through release of cytokines or reactive oxygen/nitrogen species. While this may explain the acute OL loss after E6020/TLR4 activation in the otherwise naïve spinal cord, it is still unclear what

initiates the subsequent oligodendrogenic response. It is likely not due to the presence of bare axons, as we showed previously that intraspinal TLR4 activation with LPS induces only minimal demyelination (Schonberg et al., 2007), although others have detected greater demyelination after a larger volume of LPS microinjected into spinal cord white matter (Felts et al., 2005). E6020 may induce pro-oligogenic growth factor expression in microglia directly or via crosstalk with astrocytes, as we detected elevated IL-1β and ciliary neurotrophic factor (CNTF) following intraspinal LPS injection (Schonberg et al., 2007), and others have noted an LPS-induced rise in TGFβ, LIF, IL-6, and the anti-inflammatory factor oncostatin M in the CNS (Glezer & Rivest, 2010; Jeong et al., 2013). The preferential white matter targeting of E6020-mediated macrophage activation and OL genesis may increase the therapeutic value of this agonist for boosting repair after white matter injuries in which OLs have been lost.

To examine the potential for E6020 to promote white matter repair, its ability to enhance remyelination after lysolecithin demyelination was tested. Importantly, E6020-induced TLR4 activation did not expand the area of demyelination, despite work by others showing LPS may cause prominent demyelination (Felts et al., 2005). Both lysolecithin and intraspinal TLR4 activation can cause edema, blood–brain barrier permeability and oligodendrocyte loss (Hall, 1972; Blakemore, 1976; Blakemore et al., 1977; Felts et al., 2005; Schonberg et al., 2007; Tourdias et al., 2011). However, when E6020 and lysolecithin were co-injected, OL number and edema were not different from that caused by lysolecithin alone, showing that TLR4 activation via E6020 did not exacerbate tissue pathology.

The differences in timing of macrophage activation and debris phagocytosis in lysolecithin lesions between E6020 and control groups may suggest a differential effect of E6020 in resident microglia versus peripherally derived macrophages. One would assume microglia were exposed to E6020 almost immediately after injection, yet microglial/ macrophage activation was comparable in E6020 and control groups 3 days after injection. Peripheral monocytes infiltrate lysolecithin lesions within 48 hr (Imai et al., 2008) and the earliest ones may have been activated by E6020 as its half-life is up to 40 hr (Ishizaka & Hawkins, 2007). Between day 3 and day 7, macrophage activation and myelin debris phagocytosis significantly increased in E6020 cords but did not change in salinetreated lysolecithin cords, suggesting activation of monocyte-derived macrophages may have been greater in the E6020 group compared to saline. Interestingly, although macrophage activation was delayed in the saline plus lysolecithin group, the saline group displayed significantly greater peak macrophage activation compared to the E6020 group at day 14, which may have been due to prolonged exposure to myelin debris (Clarner et al., 2012; Wang et al., 2015). Thus, TLR4 agonism by E6020 accelerated yet tempered macrophage activation after chemical demyelination.

In vitro data in this study showed that E6020 directly stimulates myelin debris uptake by macrophages. Similarly, our results show E6020 enhances macrophage myelin debris uptake *in vivo*, and promotes complete removal of lipid debris at 14–21 days after lysolecithin. In contrast, lipid debris remained significantly elevated in vehicletreated lysolecithin lesions through day 21. Recently, we showed that LPS also stimulates myelin uptake by cultured macrophages, and that TLR4 deficient mice have impaired myelin clearance after spinal

cord injury (Church et al., 2016). Central and peripheral nerve injury models have also illustrated the essential role of TLR4 signaling in clearing myelin debris (Boivin et al., 2007; Vallières et al., 2006). Notably, LPS treatment increases neutral lipid uptake by cultured human macrophages, revealing a conserved role for TLR4 signaling in this process (Napolitano, Sennato, Botham, Bordi, & Bravo, 2013). TLR4 activation of macrophages induces phagocytic programming through MyD88 and IRAK4/p38 signaling (Doyle et al., 2004). Although not assessed in this work, future studies should determine if E6020 uses a similar mechanism to induce phagocytosis. The greater than 3 day delay in phagocytosis of lipid debris relative to drug treatment is interesting since E6020 likely would have been eliminated by 3 day postinjection. Since myelin debris clearance was comparable between groups at 3 day post-injection, E6020 must have induced an early change in microglia and macrophage function that was not evident until after 3 days.

Here we show for the first time that addition of a TLR4 agonist to a CNS demyelinating lesion preserved axons and likely enhanced the amount of remyelination per OL. TLR4 signaling in macrophages has been shown to promote axonal regeneration after nerve injury both *in vitro* and *in vivo* through enhancing phagocytosis of growth inhibitory debris (Boivin et al., 2007; David & Lacroix, 2003; Rajbhandari et al., 2014). Furthermore, TLR4 mediated microglial clearance of α-synuclein is essential for limiting neurodegeneration and neuron loss in a model of multiple system atrophy (Stefanova et al., 2011). Here axon loss following chemical induced demyelination was significantly reduced by E6020. These data suggest that in addition to TLR4-mediated actions promoting axon regeneration, TLR4 signaling in macrophages also creates an environment that is protective to demyelinated CNS axons. While it has been appreciated for several years that myelin debris inhibits differentiation of OPCs into OLs, these data suggest that it may also impair the ability of OLs to extend new myelin sheaths, since E6020 and control lesions had comparable OL numbers but the E6020 group had significantly more OL-derived remyelinated axons. It is also possible that TLR4 activation concomitant with demyelination altered the macrophage response (e.g., different growth factor expression) that in turn enhanced the ability of new OLs to extend myelinating processes.

Interestingly, although E6020 microinjection into the intact spinal cord induced oligodendrogenesis, E6020 co-injection with lysolecithin-induced demyelination did not alter overall OL numbers during recovery. Comparable lesion development and chronic OL numbers after lysolecithin between E6020 treated tissue and controls indicate similar OL loss and replacement in both groups. Thus the robust oligogenic effect of E6020 in the uninjured CNS is diminished in the more complex demyelinated environment.

Our data also show TLR4 activation increased Schwann cell infiltration and remyelination in the demyelinated lesions. For decades it has been thought the astrocytic glial limitans restricts Schwann cell entry from the PNS, and their entry into the CNS occurs through compromising the glial limitans or more specifically the astrocytic processes at the dorsal root entry zone or along blood vessels, particularly in ventral and gray matter areas (Blakemore & Patterson, 1975; Franklin & Blakemore, 1993; Raine, Traugott, & Stone, 1978; Sims, Durgun, & Gilmore, 1998). Astrocytes can inhibit Schwann cell migration by disrupting integrin signaling (Afshari, Kwok, White, & Fawcett, 2010), so perhaps

intraspinal TLR4 activation alters astrocytes in a way that is more permissive to Schwann cell infiltration. An intriguing alternative possible source for the Schwann cells is from intraspinal progenitors. Recent work suggests CNS resident OPCs can differentiate into Schwann cells after a demyelinating injury (Talbott et al., 2006; Zawadzka et al., 2010) and that astrocytes play a major role in determining the balance of OPC-derived OLs vs. Schwann cells (Talbott et al., 2005; Monteiro de Castro, Deja, Ma, Zhao, & Franklin, 2015). Thus, E6020 in our study may have either recruited peripheral Schwann cells into the spinal cord and/or pushed resident OPCs toward a Schwann cell fate, with the collective outcome being increased intraspinal Schwann cell numbers and enhancement of their contribution to remyelination. Neuregulin 1 is a key regulator of Schwann cell migration, proliferation, and survival (Heermann & Schwab, 2013). Recently, systemic TLR4 activation was shown to alter neuregulin 1 expression in the brain (Yang et al., 2016), thus it is possible that TLR4 activation in the CNS can influence Schwann cell recruitment via neuregulin signaling. Our recent data implicate TLR4 signaling in regulating growth factor and cytokine expression in the damaged spinal cord (Church et al., 2016), therefore it is likely that E6020 treatment altered the inflammatory environment after lysolecithin demyelination to favor Schwann cell recruitment and survival. An alternative possibility is that the increased number of axons within the E6020 demyelinated lesions indirectly mediated the effects on Schwann cell infiltration and myelination. While lysolecithin is not typically toxic to axons when used in the concentration used here, for an unknown reason it did kill many axons in the center of the lesions. However, this serendipitously revealed that E6020 co-injected with lysolecithin reduced axon loss. Schwann cells are known to express TLR4 and release MCP-1 (CCL2) in response to damaged nerve, contributing to macrophage accumulation and Wallerian degeneration (Karanth, Yang, Yeh, & Richardson, 2006). In addition to injected E6020, putative endogenous TLR4 ligands are likely present in lysolecithin demyelination lesions similar to after spinal cord injury (Kigerl & Popovich, 2009). Thus, activation of TLR4 on recruited Schwann cells could have contributed to the accelerated accumulation of macrophages in E6020 co-injected tissue, which can infiltrate the CNS within one week of lysolecithin demyelination (Blakemore et al., 1977).

In sum, this report illustrates the importance of TLR4 signaling in promoting myelin repair, which can be achieved using a novel synthetic agonist. Specifically, E6020 accelerated myelin debris phagocytosis by macrophages, enhanced axon sparing and promoted OL and Schwann cell remyelination. Since macrophage clearance of debris is impaired with aging and contributes to decreased remyelination after CNS demyelinating injuries (Natrajan et al., 2015; Ruckh et al., 2012), data in this report indicate that selective activation of inflammation could be used to boost repair after injury and potentially enhance immune cell function in the aged CNS (for review, see Goldstein, Church, Hesp, Popovich, & McTigue, 2016). This work also sheds light on a signaling mechanism that may be involved in remyelination of central axons by peripheral myelinating cells. Lastly, these results highlight that acutely activating a single inflammatory-related receptor after demyelination can have long-term effects that alter the function of multiple cell types and change the reparative processes in the damaged adult CNS.

Acknowledgments

The authors gratefully acknowledge the excellent technical assistance of Ping Wei, Feng Qin Yin, Rochelle Deibert, Wenmin Lai, Angela Blissett and the OSU Campus Microscopy and Imaging Facility. The E6020 was generously provided by Eisai, Inc. This work was funded by R01-NS082095 (DMM), P30-NS045758 (DMM), the Ray W. Poppleton Endowment (PGP), and the Center for Brain and Spinal Cord Repair.

Funding information

Grant numbers: R01-NS082095, P30-NS045758; Ray W. Poppleton Endowment and the Center for Brain and Spinal Cord Repair.

References

Blakemore WF. Invasion of Schwann cells into the spinal cord of the rat following local injections of lysolecithin. Neuropathology and Applied Neurobiology. 1976; 2:21–39.

Blakemore WF, Eames RA, Smith KJ, McDonald WI. Remyelination in the spinal cord of the cat following intraspinal injections of lysolecithin. Journal of Neurological Sciences. 1977; 33:31–43.

Afshari FT, Kwok JC, White L, Fawcett JW. Schwann cell migration is integrin-dependent and inhibited by astrocyte-produced aggrecan. Glia. 2010; 57:857–869.

Blakemore WF, Patterson RC. Observations on the interactions of Schwann cells and astrocytes following X-irradiation of neonatal rat spinal cord. Journal of Neurocytology. 1975; 4:573–585. [PubMed: 1177001]

Blomkalns AL, Gavrila D, Thomas M, Neltner BS, Blanco VM, Benjamin S, Weintraub NL. CD14 directs adventitial macrophage precursor recruitment: Role in early abdominal aortic aneurysm formation. Journal of American Heart Association. 2013; 2:e000065.

Boivin A, Pineau I, Barrette B, Filali M, Vallieres N, Rivest S, Lacroix S. Toll-Like receptor signaling is critical for Wallerian degeneration and functional recovery after peripheral nerve injury. Journal of Neuroscience. 2007; 27:12565–12576. [PubMed: 18003835]

Bruück W, Porada P, Poser S, Rieckmann P, Hanefeld F, Kretzschmar HA, Lassmann H. Monocyte/macrophage differentiation in early multiple sclerosis lesions. Annals of Neurology. 1995; 38:788–796. [PubMed: 7486871]

Burgess AW, Metcalf D, Kozka IJ, Simpson RJ, Vairo G, Hamilton JA, Nice EC. Purification of two forms of colony-stimulating factor from mouse L-cell-conditioned medium. Journal of Biological Chemistry. 1985; 260:16004–16011. [PubMed: 3877728]

Church JS, Kigerl KA, Lerch JK, Popovich PG, McTigue DM. TLR4 deficiency impairs oligodendrocyte formation in the injured spinal cord. Journal of Neuroscience. 2016; 36:6352–6364. [PubMed: 27277810]

Clarner T, Diederichs F, Berger K, Denecke B, Gan L, van der Valk P, Beyer C, Kipp M. Myelin debris regulates inflammatory responses in an experimental demyelination animal model and multiple sclerosis lesions. Glia. 2012; 60:1468–1480. [PubMed: 22689449]

Coley JS, Calderon TM, Gaskill PJ, Eugenin EA, Berman JW. Dopamine increases CD14+CD16+ monocyte migration and adhesion in the context of substance abuse and HIV neuropathogenesis. PLoS ONE. 2015; 10:e0117450. [PubMed: 25647501]

David S, Lacroix S. Molecular approaches to spinal cord repair. Annual Review of Neuroscience. 2003; 26:411–440.

Doyle SE, O'Connell RM, Miranda GA, Vaidya SA, Chow EK, Liu P, Cheng G. Toll-like receptors induce a phagocytic gene program through p38. Journal of Experimental Medicine. 2004; 199:81–90. [PubMed: 14699082]

Felts PA, Woolston A-M, Fernando HB, Asquith S, Gregson NA, Mizzi OJ, Smith KJ. Inflammation and primary demyelination induced by the intraspinal injection of lipopolysaccharide. Brain. 2005; 128:1649–1666. [PubMed: 15872019]

Franklin RJ, Blakemore WF. Requirements for Schwann cell migration within CNS environments: A viewpoint. International Journal of Developmental Neuroscience. 1993; 11:641–649. [PubMed: 8116476]

Glezer I. Innate immunity triggers oligodendrocyte progenitor reactivity and confines damages to brain injuries. Faseb Journal. 2006; 20:750–752. [PubMed: 16464958]

Glezer I, Rivest S. Oncostatin M is a novel glucocorticoid-dependent neuroinflammatory factor that enhances oligodendrocyte precursor cell activity in demyelinated sites. Brain Behavior and Immunity. 2010; 24:695–704.

Goldstein EZ, Church JS, Hesp ZC, Popovich PG, McTigue DM. A silver lining of neuroinflammation: Beneficial effects on myelination. Experimental Neurology. 2016; 283:550–559. [PubMed: 27151600]

Graça DL, Blakemore WF. Delayed remyelination in rat spinal cord following ethidium bromide injection. Neuropathology and Applied Neurobiology. 1986; 12:593–605. [PubMed: 3561693]

Hall SM. The effect of injections of lysophosphatidyl choline into white matter of the adult mouse spinal cord. Journal of Cellular Science. 1972; 10:535–546.

Hall SM, Gregson NA. The in vivo and ultrastructural effects of injection of lysophosphatidyl choline into myelinated peripheral nerve fibres of the adult mouse. Journal of Cellular Science. 1971; 9:769–789.

Heermann S, Schwab MH. Molecular control of Schwann cell migration along peripheral axons: Keep moving! Cellular Adhesion & Migration. 2013; 7:18–22.

Hendrickx DAE, Schuurman KG, van Draanen M, Hamann J, Huitinga I. Enhanced uptake of multiple sclerosis-derived myelin by THP-1 macrophages and primary human microglia. Journal of Neuroinflammation. 2014; 11:64. [PubMed: 24684721]

Imai M, Watanabe M, Suyama K, Osada T, Sakai D, Kawada H, Mochida J. Delayed accumulation of activated macrophages and inhibition of remyelination after spinal cord injury in an adult rodent model. Journal of Neurosurgery: Spine. 2008; 8:58–66. [PubMed: 18173348]

Ishizaka ST, Hawkins LD. E6020: A synthetic Toll-like receptor 4 agonist as a vaccine adjuvant. Expert Review of Vaccines. 2007; 6:773–784. [PubMed: 17931157]

Janova H, Boöttcher C, Holtman IR, Regen T, van Rossum D, Goötz A, Hanisch U-K. CD14 is a key organizer of microglial responses to CNS infection and injury. Glia. 2015; 64:635–649. [PubMed: 26683584]

Jeffery ND, Blakemore WF. Remyelination of mouse spinal cord axons demyelinated by local injection of lysolecithin. Journal of Neurocytology. 1995; 24:775–781. [PubMed: 8586997]

Jeong HK, Ji KM, Kim J, Jou I, Joe EH. Repair of astrocytes, blood vessels, and myelin in the injured brain: Possible roles of blood monocytes. Molecular Brain. 2013; 6:28. [PubMed: 23758980]

Karanth S, Yang G, Yeh J, Richardson PM. Nature of signals that initiate the immune response during Wallerian degeneration of peripheral nerves. Experimental Neurology. 2006; 202:161–166. [PubMed: 16828744]

Kigerl, KA., Popovich, PG. Current Topics in Microbiology and Immunology. Vol. 336. Berlin, Heidelberg: Springer; 2009. Toll-like receptors in spinal cord injury; p. 121-136.

Kotter MR, Li W-W, Zhao C, Franklin RJM. Myelin impairs CNS remyelination by inhibiting oligodendrocyte precursor cell differentiation. Journal of Neuroscience. 2006; 26:328–332. [PubMed: 16399703]

Kotter MR, Setzu A, Sim FJ, van Rooijen N, Franklin RJM. Macrophage depletion impairs oligodendrocyte remyelination following lysolecithin-induced demyelination. Glia. 2001; 35:204–212. [PubMed: 11494411]

Kotter MR, Zhao C, van Rooijen N, Franklin RJM. Macrophage-depletion induced impairment of experimental CNS remyelination is associated with a reduced oligodendrocyte progenitor cell response and altered growth factor expression. Neurobiology of Disease. 2005; 18:166–175. [PubMed: 15649707]

Lampron A, Larochelle A, Laflamme N, Prefontaine P, Plante MM, Sanchez MG, Rivest S. Inefficient clearance of myelin debris by microglia impairs remyelinating processes. Journal of Experimental Medicine. 2015; 212:481–495. [PubMed: 25779633]

Lehnardt S, Lachance C, Patrizi S, Lefebvre S, Follett PL, Jensen FE, Vartanian T. The toll-like receptor TLR4 is necessary for lipopolysaccharide-induced oligodendrocyte injury in the CNS. Journal of Neuroscience. 2002; 22:2478–2486. [PubMed: 11923412]

Li HJ, Zhang X, Zhang F, Wen XH, Lu LJ, Shen J. Enhanced repair effect of Toll-like receptor 4 activation on neurotmesis: assessment using MR neurography. American Journal of Neuroradiology. 2014; 35:1608–1614. [PubMed: 24874529]

Lindvall O, Bjoörklund A, Skagerberg G. Dopamine-containing neurons in the spinal cord: Anatomy and some functional aspects. Annals of Neurology. 1983; 14:255–260. [PubMed: 6314870]

Longbrake EE, Lai W, Ankeny DP, Popovich PG. Characterization and modeling of monocyte-derived macrophages after spinal cord injury. Journal of Neurochemistry. 2007; 102:1083–1094. [PubMed: 17663750]

Lu Y-C, Yeh W-C, Ohashi PS. LPS/TLR4 signal transduction pathway. Cytokine. 2008; 42:145–151. [PubMed: 18304834]

Ma M, Wei T, Boring L, Charo IF, Ransohoff RM, Jakeman LB. Monocyte recruitment and myelin removal are delayed following spinal cord injury in mice with CCR2 chemokine receptor deletion. Journal of Neuroscience Research. 2002; 68:691–702. [PubMed: 12111830]

McTigue DM, Wei P, Stokes BT. Proliferation of NG2-positive cells and altered oligodendrocyte numbers in the contused rat spinal cord. Journal of Neurosciene. 2001; 21:3392–3400.

Monteiro de Castro G, Deja NA, Ma D, Zhao C, Franklin RJM. Astrocyte activation via Stat3 signaling determines the balance of oligodendrocyte versus Schwann cell remyelination. The American Journal of Pathology. 2015; 185:2431–2440. [PubMed: 26193667]

Morefield GL, Hawkins LD, Ishizaka ST, Kissner TL, Ulrich RG. Synthetic Toll-like receptor 4 agonist enhances vaccine efficacy in an experimental model of toxic shock syndrome. Clinical and Vaccine Immunology. 2007; 14:1499–1504. [PubMed: 17715328]

Napolitano M, Sennato S, Botham KM, Bordi F, Bravo E. Role of macrophage activation in the lipid metabolism of postprandial triacylglycerol-rich lipoproteins. Experimental Biology Medicine (Maywood). 2013; 238:98–110.

Natrajan MS, la Fuente de AG, Crawford AH, Linehan E, Nunñez V, Johnson K, Franklin RJM. Retinoid X receptor activation reverses age-related deficiencies in myelin debris phagocytosis and remyelination. Brain. 2015; 138:3581–3597. [PubMed: 26463675]

Neumann H, Kotter MR, Franklin RJM. Debris clearance by microglia: An essential link between degeneration and regeneration. Brain. 2008; 132:288–295. [PubMed: 18567623]

Norton WT, Poduslo SE. Myelination in rat brain: Method of myelin isolation. Journal of Neurochemistry. 1973; 21:749–757. [PubMed: 4271082]

Pang Y, Cai ZW, Rhodes PG. Effects of lipopolysaccharide on oligodendrocyte progenitor cells are mediated by astrocytes and microglia. Journal of Neuroscience Research. 2000; 62:510–520. [PubMed: 11070494]

Pang Y, Campbell L, Zheng B, Fan L, Cai Z, Rhodes P. Lipo-polysaccharide-activated microglia induce death of oligodendrocyte progenitor cells and impede their development. Neuroscience. 2010; 166:464–475. [PubMed: 20035837]

Raine CS, Traugott U, Stone SH. Glial bridges and Schwann cell migration during chronic demyelination in the CNS. Journal of Neurocytology. 1978; 7:541–553. [PubMed: 722315]

Rajbhandari L, Tegenge MA, Shrestha S, Ganesh Kumar N, Malik A, Mithal A, Venkatesan A. Toll-like receptor 4 deficiency impairs microglial phagocytosis of degenerating axons. Glia. 2014; 253:102–110.

Robinson S, Miller RH. Contact with central nervous system myelin inhibits oligodendrocyte progenitor maturation. Developmental Biology. 1999; 216:359–368. [PubMed: 10588885]

Ruckh JM, Zhao J-W, Shadrach JL, van Wijngaarden P, Rao TN, Wagers AJ, Franklin RJM. Rejuvenation of regeneration in the aging central nervous system. Cell Stem Cell. 2012; 10:96–103. [PubMed: 22226359]

Schmittgen TD, Livak KJ. Analyzing real-time PCR data by the comparative CT method. Nature Protocol. 2008; 3:1101–1108.

Schonberg DL, McTigue DM. Iron is essential for oligoden-drocyte genesis following intraspinal macrophage activation. Experimental Neurology. 2009; 218:64–74. [PubMed: 19374902]

Schonberg DL, Popovich PG, McTigue DM. Oligodendrocyte generation is differentially influenced by toll-like receptor (TLR) 2 and TLR4-mediated intraspinal macrophage activation. Journal of Neuropathology and Experimental Neurology. 2007; 66:1124–1135. [PubMed: 18090921]

Sims TJ, Durgun MB, Gilmore SA. Schwann cell invasion of ventral spinal cord: The effect of irradiation on astrocyte barriers. Journal of Neuropathology and Experimental Neurology. 1998; 57:866–873. [PubMed: 9737550]

Stefanova N, Fellner L, Reindl M, Masliah E, Poewe W, Wenning GK. Toll-like receptor 4 promotes α-synuclein clearance and survival of nigral dopaminergic neurons. American Journal of Pathology. 2011; 179:954–963. [PubMed: 21801874]

Talbott JF, Cao Q, Enzmann GU, Benton RL, Achim V, Cheng XX, Whittemore SR. Schwann cell-like differentiation by adult oligodendrocyte precursor cells following engraftment into the demyelinated spinal cord is BMP-dependent. Glia. 2006; 54:147–159. [PubMed: 16921543]

Talbott JF, Loy DN, Liu Y, Qiu MS, Bunge MB, Rao MS, Whittemore SR. Endogenous Nkx2.2+/Olig2+ oligodendro-cyte precursor cells fail to remyelinate the demyelinated adult rat spinal cord in the absence of astrocytes. Experimental Neurology. 2005; 192:11–24. [PubMed: 15698615]

Tourdias T, Mori N, Dragonu I, Cassagno N, Boiziau C, Aussudre J, Dousset V. Differential aquaporin 4 expression during edema build-up and resolution phases of brain inflammation. Journal of Neuroinflammation. 2011; 8:143. [PubMed: 22011386]

Triarhou LC, Herndon RM. Effect of macrophage inactivation on the neuropathology of lysolecithin-induced demyelination. British Journal of Experimental Pathology. 1985; 66:293. [PubMed: 4005147]

Vallières N, Berard JL, David S, Lacroix S. Systemic injections of lipopolysaccharide accelerates myelin phagocytosis during Wallerian degeneration in the injured mouse spinal cord. Glia. 2006; 53:103–113. [PubMed: 16206158]

Wang X, Cao K, Sun X, Chen Y, Duan Z, Sun L, Ren Y. Macrophages in spinal cord injury: Phenotypic and functional change from exposure to myelin debris. Glia. 2015; 63:635–651. [PubMed: 25452166]

Watanabe M, Toyama Y, Nishiyama A. Differentiation of proliferated NG2-positive glial progenitor cells in a remyelinating lesion. Journal of Neuroscience Research. 2002; 69:826–836. [PubMed: 12205676]

Yang Z, Jiang Q, Chen SX, Hu CL, Shen HF, Huang PZ, Zhao WJ. Differential changes in Neuregulin-1 signaling in major brain regions in a lipopolysaccharide-induced neuroinflammation mouse model. Molecular Medicine Reports. 2016; 14:790–796. [PubMed: 27220549]

Zawadzka M, Rivers LE, Fancy SPJ, Zhao C, Tripathi R, Jamen F, Franklin RJM. CNS-resident glial progenitor/stem cells produce Schwann cells as well as oligodendrocytes during repair of CNS demyelination. Cell Stem Cell. 2010; 6:578–590. [PubMed: 20569695]

Zhang F, Yao SY, Whetsell WO, Sriram S. Astrogliopathy and oligodendrogliopathy are early events in CNS demyelination. Glia. 2013; 61:1261–1273. [PubMed: 23832594]

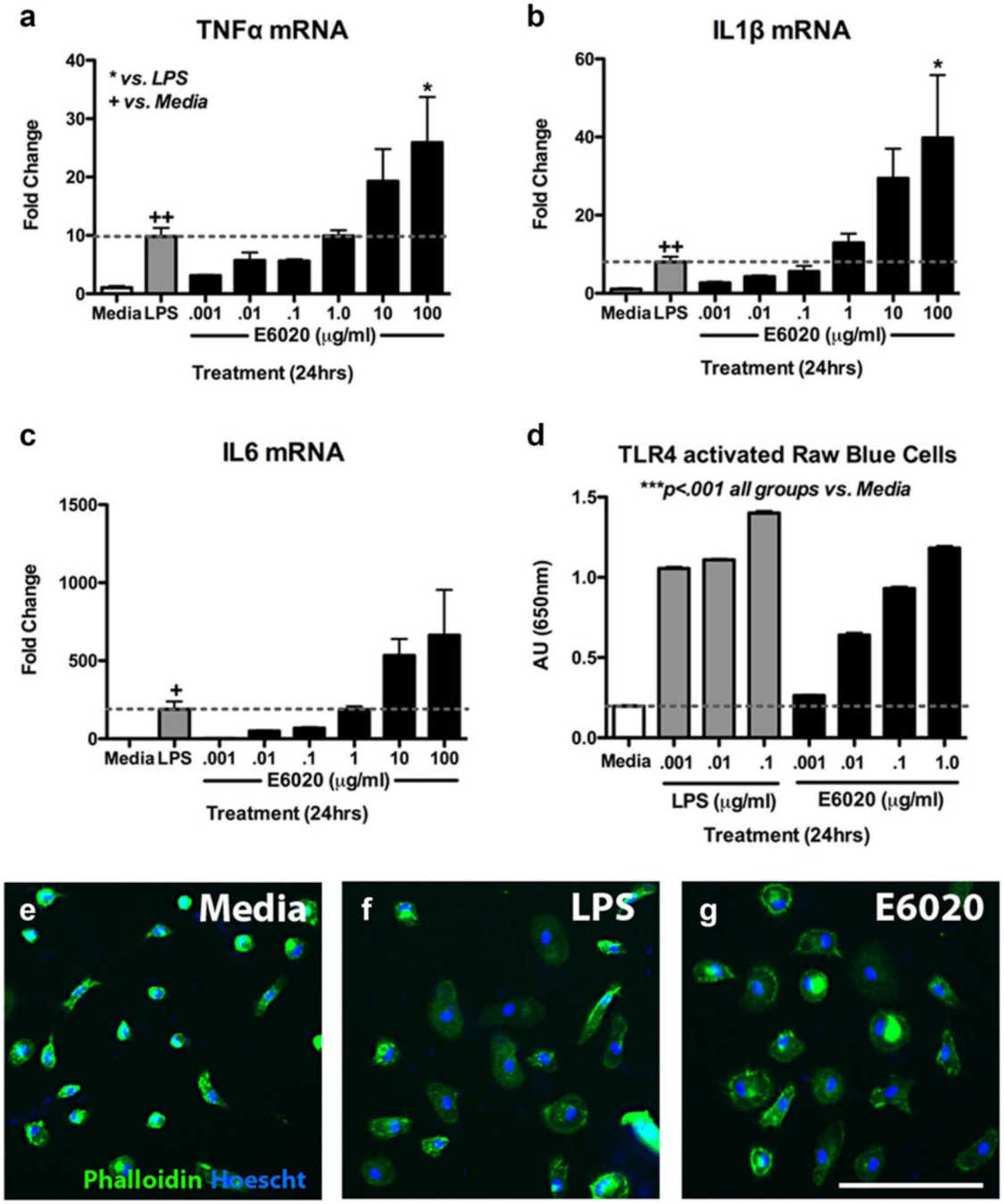

FIGURE 1.

E6020 activated BMDMs similar to LPS. (a–c) 24 hr treatment of rat BMDMs with LPS (0.1 μg/mL, gray bars) significantly increased expression of TNFα, IL-1β, and IL-6 over media treatment (white bars). 24 hr treatment of increasing E6020 doses showed similar expression between LPS treatment and a 10× higher E6020 treatment (1 μg/mL, black bars); dotted line represents LPS-fold change of gene expression. (d) Raw Blue Cells (macrophages) treated with increasing doses of LPS (gray bars) or E6020 (black bars) had significantly higher NF-κB/AP-1 activation compared to media treatment (white bar) as measured using QUANTI-

Blue. (e–g) Phalloidin stain (green) shows morphology of BMDMs counterstained with Hoescht (blue) treated with media (e), LPS (0.1 μg/mL) (f), or E6020 (1 μg/mL) (g) for 24 hr. LPS and E6020 induced a larger more rounded cell body typical of an activated macrophage, compared to the small rounded or bipolar morphology in the media-treated group. *p <.05 vs. LPS; ^{+}p <.05, ^{++}p <.01 versus media (a–c). Scale bar = 100 μm (e–g). Data are mean-± SEM. [Color figure can be viewed at wileyonlinelibrary.com]

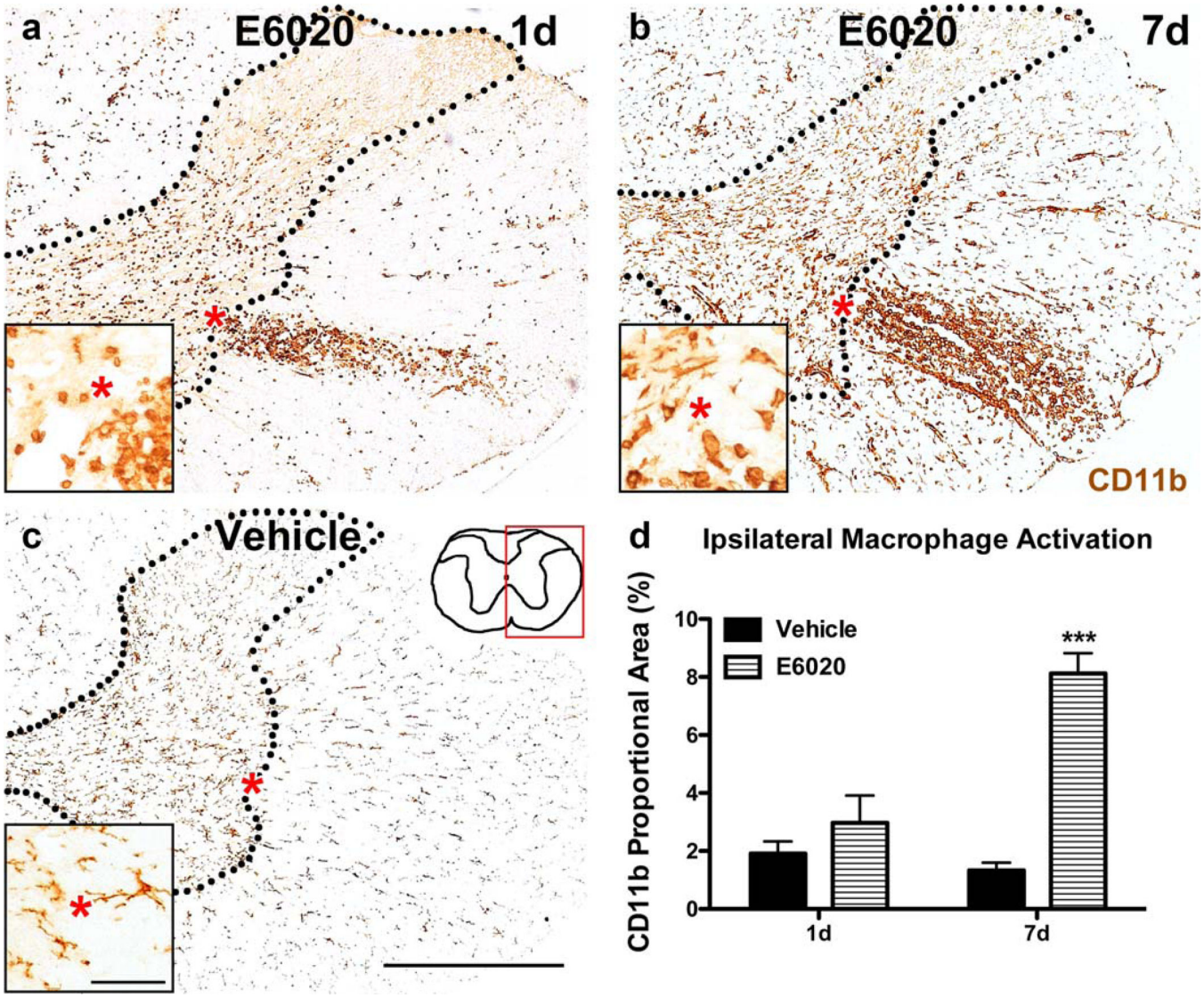

FIGURE 2.

E6020 microinjection (MI) at the GM/WM border activated intraspinal macrophages. (a) Activated macrophages in the GM and WM were present in E6020 MI tissue at day 1. (b) Overall CD11b immunoreactivity increased between day 1 and day 7 after E6020 MI. At both times, an oval shaped accumulation of activated macrophages was present in the lateral WM. (c) CD11b immunoreactivity in vehicle-treated tissue displayed resting microglia morphology at day 1 and day 7 (pictured here). Red box on spinal cord schematic (c) outlines area of representative images. Insets show high power of GM/WM border for each treatment. Red asterisks denote same area in regular and high power images. (d) Proportional area quantification of CD11b immunoreactivity in the ipsilateral spinal cord showed increased macro-phage activation with E6020 MI (striped bars) at day 7 compared to vehicle (black bars). ***p <.001 versus vehicle. Scale bar 5500 μm (a– c); 50 μm (insets, a–c). Data are mean ± SEM. [Color figure can be viewed at wileyonlinelibrary.com]

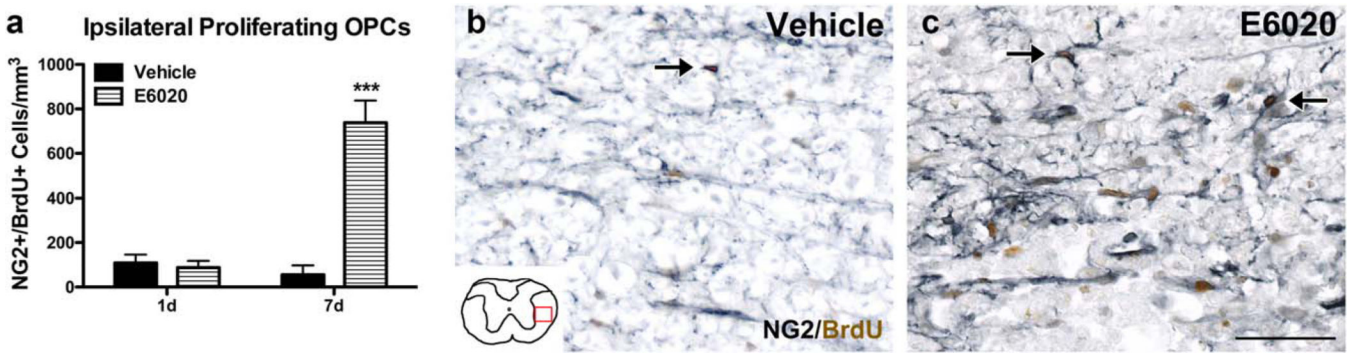

FIGURE 3.

E6020 microinjection (MI) induced intraspinal OPC proliferation. (a) Quantification of NG2+/BrdU+ cells in the ipsilateral spinal cord. On day 1 animals received BrdU at 1, 2, and 4 hr post-MI; on day 7 animals received BrdU at 1 hr post-MI and daily through 7 days. At day 1 post-MI, there were few BrdU+ NG2 cells, but by day 7, E6020-treated tissue (striped bars) had significantly more dividing OPCs than the vehicle group (black bars). Representative images of NG2 (gray)/BrdU (brown) immunohistochemistry at day 7 in vehicle (b) and E6020 tissue (c) in the lateral WM show many BrdU+ cells (arrows) adjacent to the injection site after TLR4 agonist but not vehicle treatment. Red box on schematic (b) outlines location of representative images. ***p <.001 vs. vehicle. Scale bars = 50 μm (b, c). Data are mean ± SEM. [Color figure can be viewed at wileyonlinelibrary.com]

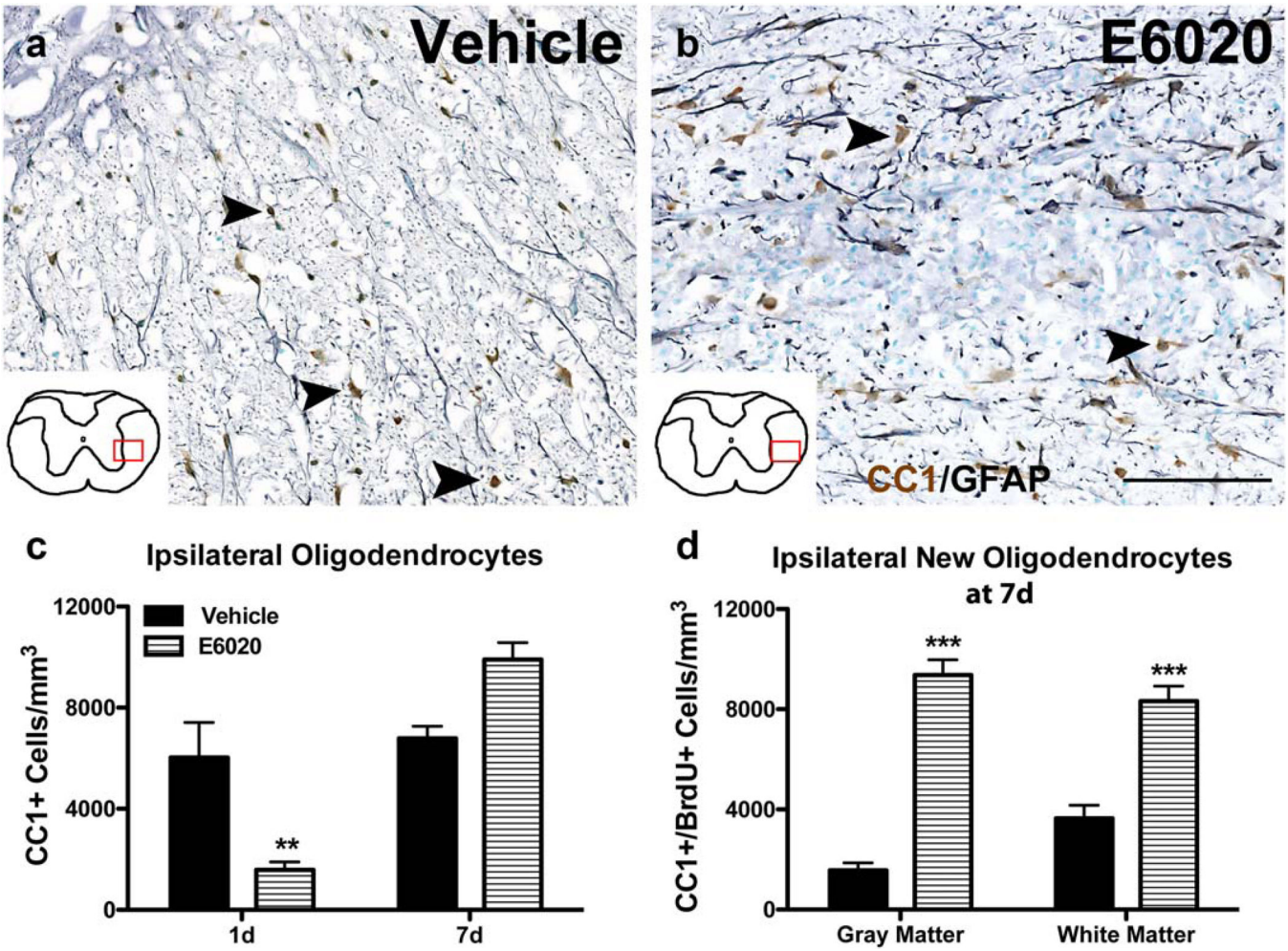

FIGURE 4.

Oligodendrocytes are lost and replaced following E6020 microinjection (MI). Representative images of oligodendrocytes (CC1, brown) and astrocytes (GFAP, gray) counterstained with methyl green at the injection site at 7 days after vehicle (a) and E6020 MI (b). Arrowheads indicate CC1+ oligodendrocytes. Red box over spinal cord schematics outline where representative images were taken. (c) Quantification of CC1+ oligodendrocytes in the ipsilateral half showed oligodendrocyte loss 1 day after E6020 MI (striped bars) compared to vehicle (black bars), and a rebound in oligodendrocyte numbers slightly beyond baseline at 7 days. (d) BrdU+ oligodendrocytes were counted in the gray and white matter at the injection site 7 days post-MI from animals receiving BrdU at 1 hr and 1–7 days. In both gray and white matter regions, the E6020 group (striped bars) had significantly more new oligodendrocytes compared to vehicle (black bars). $^{**}p < .01$, $^{***}p < .001$ versus vehicle. Scale bar = 100 μm (a, b). Data are mean ± SEM. [Color figure can be viewed at wileyonlinelibrary.com]

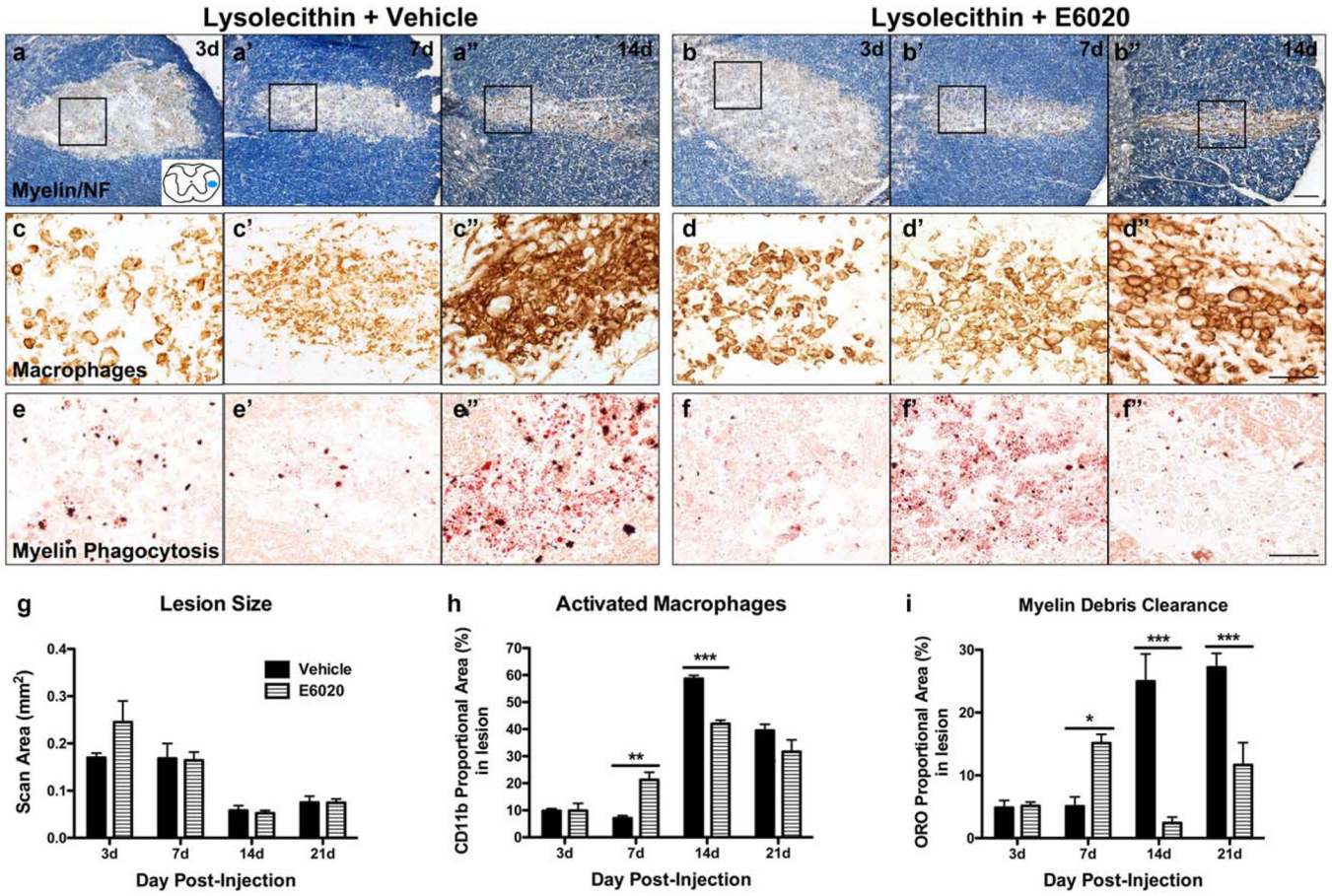

FIGURE 5.

E6020 accelerates macrophage activation and myelin debris clearance after lysolecithin-induced demyelination. (a, b) Demyeli-nated lesions were revealed by myelin stain with EC (blue) and axon immunolabeling with anti-NF at day 3 (a, b), day 7 (a', b'), and day 14 (a", b") in animals co-injected with vehicle (a) or E6020 (b). Spinal cord schematic (a) outlines area of demyelination in lateral white matter (blue oval). Acutely after lysolecithin, both groups show demyelination (lack of EC stain) and slight edema. Over the course of 2 weeks, edema resolves and lesions shrink. E6020 did not alter lesion size at any time. (c, d) CD11b immunoreactivity at the same time points and from the same representative animals in a and b (area outlined with black box) demonstrates increased macrophage activation between 3 and 14 days postinjection in vehicle (c, c', c") and E6020 (d, d', d") groups. E6020 treatment induced greater macrophage reactivity at day 7 (d') and day 14 (d"), while vehicletreated animals had significantly greater macrophage activation at day 14 (c") compared to E6020. (e, f) Myelin debris phagocytosis measured with oil red O stain from the same representative animals in a and b (area outlined with black box) shows that E6020 accelerates myelin debris clearance. Oil red O is significantly greater at day 7 after E6020 treatment (f) compared to vehicle (e') and is cleared from the lesion by day 14 (f") at the time when staining is the highest with vehicle (e"). Quantification of (g) lesion size (EC/NF), (h) macrophage activation (CD11b), and (i) myelin debris clearance (oil red O stain) at 3, 7, 14, and 21 days post-lysolecithin plus vehicle (black bars) or E6020 (striped bars) co-

injection. *$p < .05$, **$p < .01$, ***$p < .001$ versus vehicle. Scale bars = 100 μm (a, b), 50 μm (c–f). Data are mean ±SEM. [Color figure can be viewed at wileyonlinelibrary.com]

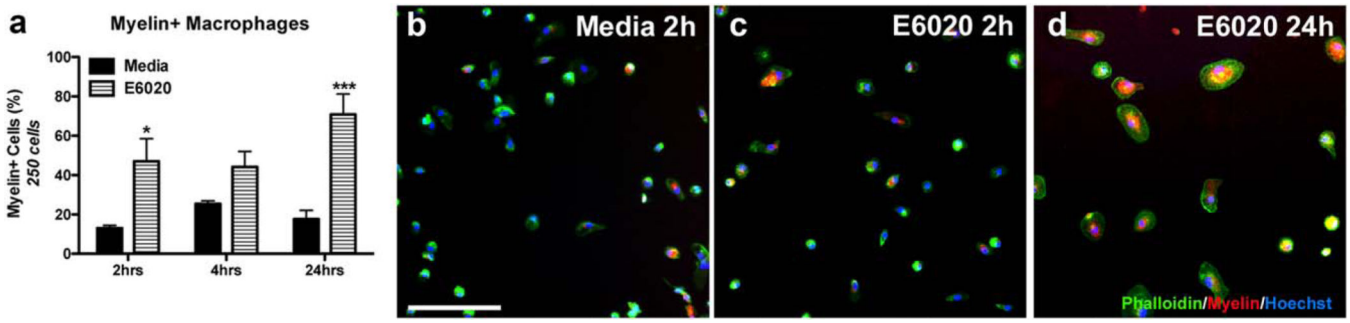

FIGURE 6.

E6020 increased myelin phagocytosis by BMDMs. (a) Quantification of myelin-containing rat BMDMs treated with pHrodo Red tagged rat myelin and Media or E6020 (1 μg/mL) for 2, 4, or 24 hr *in vitro*. (b–d) High power representative images of Media (b, 2h) and E6020 (c, 2 hr; d, 24 hr) treatment showing Phalloidin+ BMDMs (green) containing myelin (red) with nuclear counterstain Hoechst (blue). *$p < .05$, ***$p < .001$ versus Media. Scale bar = 100 μm (b–d). Data are mean ±SEM. [Color figure can be viewed at wileyonlinelibrary.com]

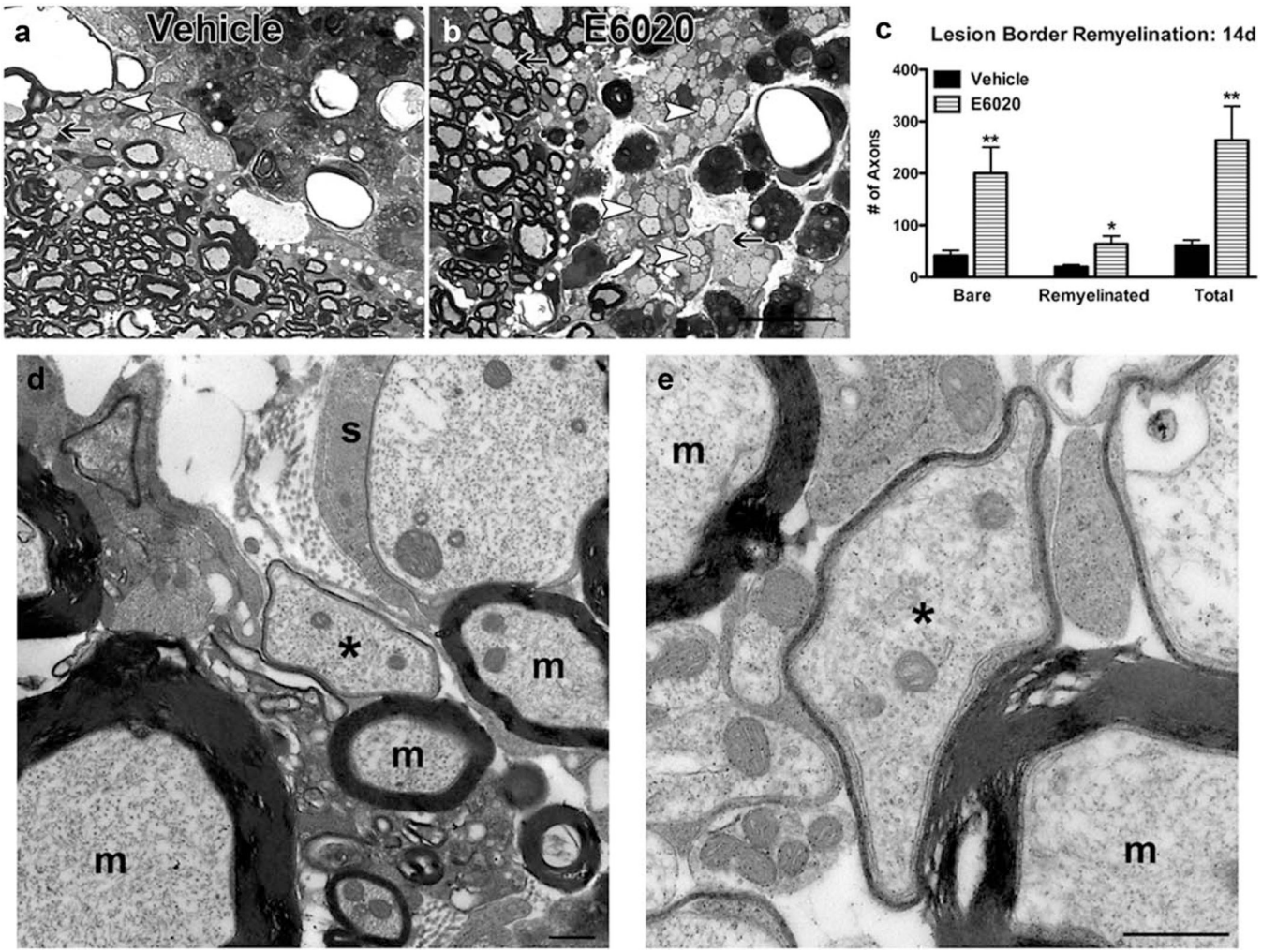

FIGURE 7.

E6020 increased axon survival and remyelination after lysolecithin-induced demyelination. (a, b) Semithin plastic tissue was prepared from spinal cords 14 days after injection of lysolecithin plus vehicle (a) or E6020 (b). White dotted lines delineate lesion border. Arrows indicate bare axons, and arrowheads indicate thinly remyelinated axons. (c) Quantification of bare axons and thinly myelinated axons indicative of oligodendrocyte remyelination along the lesion border. E6020 treated tissue (striped bars) had significantly more bare, remyelinated, and total axons compared to vehicle (black bars) at day 14, indicating increased axon survival and remyelination. (d, e) Electron microscopy imaging confirms thin myelin profiles seen in (b) are myelin wraps indicative of oligodendrocyte remyelination. Asterisks (*) indicate remyelinated axons and ‘m’ indicates axons with spared myelinated. A putative Schwann cell (s) wrapping an axon is present in D. Scale bars = 20 μm (a, b), 500 nm (d, e). Data are mean ±SEM

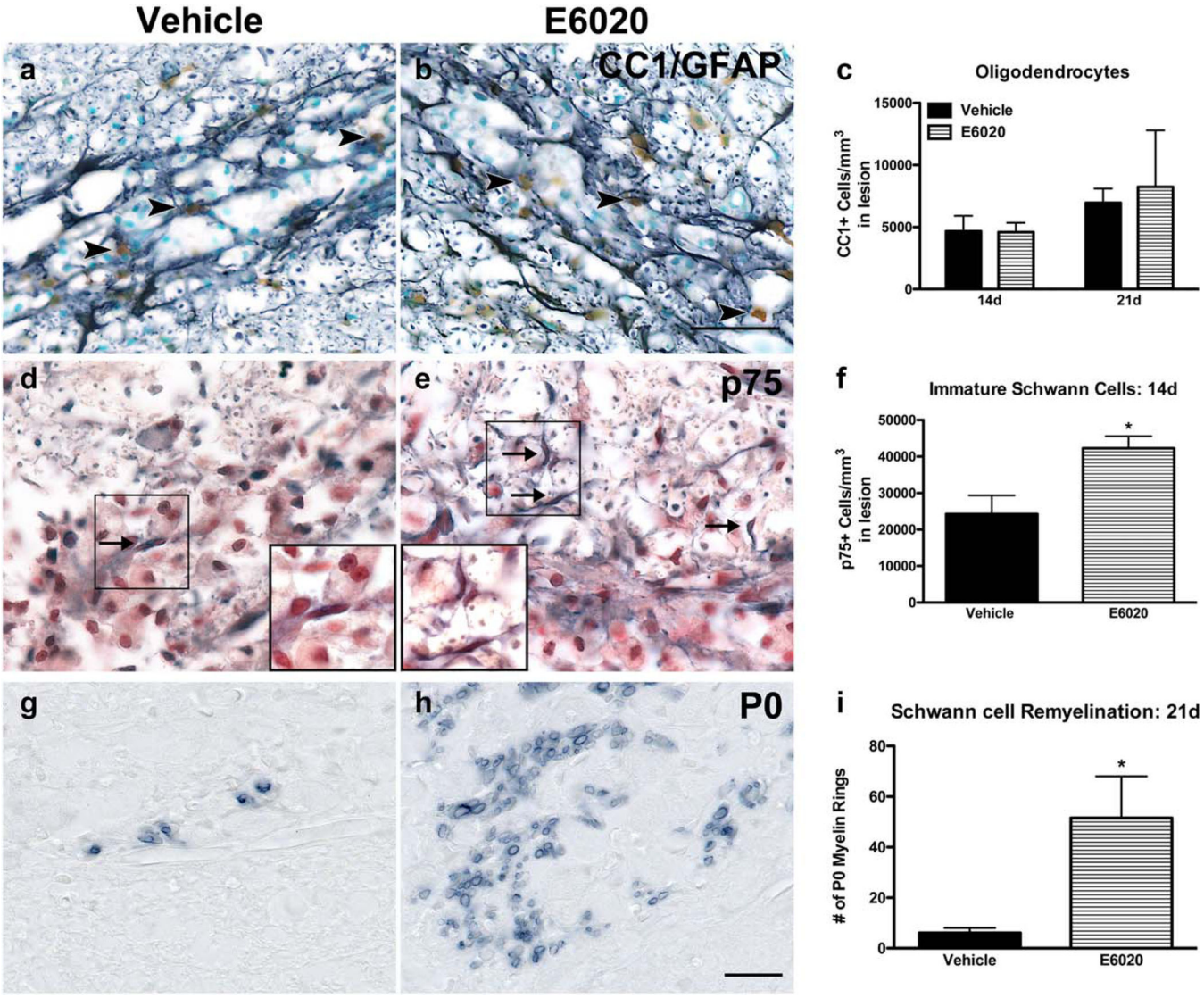

FIGURE 8.

E6020 increased Schwann cell remyelination but did not alter oligodendrocyte number after lysolecithin-induced demyelination. (a, b) Representative images of oligodendrocytes (CC1, brown) and astrocytes (GFAP, black) in vehicle (a) or E6020 (b) co-injected lesions at 21 days postinjection. Arrowheads indicate CC1+ oligodendrocytes. (c) Quantification within lesions at 14 and 21 days postinjection showed no difference in oligodendrocyte number between groups. (d, e) Immature, nonmyelinating Schwann cells were quantified as p75+ cells in vehicle (d) and E6020 (e) treated animals at 14 days postinjection. Arrows indicate p75+ Schwann cells. High power insets show examples of p75+ cells. (f) E6020 (striped bar) concomitant with lysolecithin increased the number of p75+ cells within the demyelinated lesions at 14 days compared to vehicle (black bar). (g, h) Representative images of P0+ Schwann cell myelin in vehicle (G; black bar) and E6020 (h; striped bar) treated tissue at 21 days postinjection. (i) Quantification of P0+ myelin rings showed more myelin rings with E6020 treatment (striped bar) compared to vehicle (black bar). *$p < .05$, **$p < .01$ vs.

vehicle. Scale bars = 50 μm (a, b), 20 μm (d, e, g, h). Data are mean ± SEM. [Color figure can be viewed at wileyonlinelibrary.com]

TABLE 1

Forward and reverse primer sequences for real time PCR

Rat gene	Forward primer (5′–3′)	Reverse primer (5′–3′)
18s	TTCGGAACTGAGGCCATGAT	TTTCGCTCTGGTCCGTCTTG
lL1β	GAAGATGGAAAAGCGGTTTG	AACTATGTCCCGACCATTGC
IL6	CTGGAGTTCCGTTTCTACCTGG	TGGTCCTTAGCCACTCCTTCTG
TNFα	TGATCCGAGATGTGGAACTGG	CGATCACCCCGAAGTTCAGTAG

IL, interleukin; TNF, tumor necrosis factor.